Database of novel magnetic materials for high-performance permanent magnet development

P. Nieves [a, *], S. Arapan [a, b], J. Maudes-Raedo [c], R. Marticorena-Sánchez [c], N.L. Del Brío [a], A. Kovacs [d],
C. Echevarria-Bonet [e], D. Salazar [e], J. Weischenberg [f], H. Zhang [f], O.Yu. Vekilova [g], R. Serrano-López [a],
J.M. Barandiaran [e], K. Skokov [f], O. Gutfleisch [f], O. Eriksson [g, h], H.C. Herper [g], T. Schrefl [d], S. Cuesta-López [a, i]

[a] ICCRAM, International Research Center in Critical Raw Materials and Advanced Industrial Technologies, Universidad de Burgos, 09001 Burgos, Spain
[b] VSB Tech Univ Ostrava, IT4Innovations, 17 Listopadu 15, CZ-70833 Ostrava, Czech Republic
[c] Department of Civil Engineering, Universidad de Burgos, 09006 Burgos, Spain
[d] Center for Integrated Sensor Systems, Danube University Krems, Lower Austria, 3500 Krems, Austria
[e] BCMaterials, Basque Centre for Materials, Applications and Nanostructures, UPV/EHU Science Park, 48940 Leioa, Spain
[f] Department of Materials and Geosciences, TU Darmstadt, Darmstadt 64287, Germany
[g] Department of Physics and Astronomy, Uppsala University, Box 516, 75121 Uppsala, Sweden
[h] School of Science and Technology, Örebro University, SE-70182 Örebro, Sweden
[i] ICAMCyL Foundation International Center for Advanced Materials and Raw Materials of Castilla y León, 24492 Cubillos del Sil, León, Spain

ARTICLE INFO

ABSTRACT

This paper describes the open Novamag database that has been developed for the design of novel Rare-Earth free/lean permanent magnets. Its main features as software technologies, friendly graphical user interface, advanced search mode, plotting tool and available data are explained in detail. Following the philosophy and standards of Materials Genome Initiative, it contains significant results of novel magnetic phases with high magnetocrystalline anisotropy obtained by three computational high-throughput screening approaches based on a crystal structure prediction method using an Adaptive Genetic Algorithm, tetragonally distortion of cubic phases and tuning known phases by doping. Additionally, it also includes theoretical and experimental data about fundamental magnetic material properties such as magnetic moments, magnetocrystalline anisotropy energy, exchange parameters, Curie temperature, domain wall width, exchange stiffness, coercivity and maximum energy product, that can be used in the study and design of new promising high-performance Rare-Earth free/lean permanent magnets. The results therein contained might provide some insights into the ongoing debate about the theoretical performance limits beyond Rare-Earth based magnets. Finally, some general strategies are discussed to design possible experimental routes for exploring most promising theoretical novel materials found in the database.

1. Introduction

Permanent magnets (PMs) are materials with an internal structure capable of creating an external magnetic field by themselves. Nowadays, these materials play an important role in critical sectors of our advanced society as transport, energy, information and communications technology [1]. The magnetic field source given by PMs is widely used in many technological applications, e.g. for inducing mechanical motion in electric motors, making sound in loudspeakers, generating electrical energy in wind turbines, data storage in computer engineer-

ing, magnetic resonance imaging in healthcare industry, holding, oil dewaxing, etc [2,3]. In many of these technologies, most efficient designs are frequently achieved using PMs. For instance, the omission of gearboxes in wind turbines based on PM generators considerably reduces maintenance, service costs and overall material utilization [4]. Similarly, PM-based motors have many advantages compared to internal combustion engines including high efficiency, compact size, light weight, and high torque [1].

At macroscopic scale, a magnet is described by extrinsic properties that are deduced from the hysteresis loop and determine its perfor-
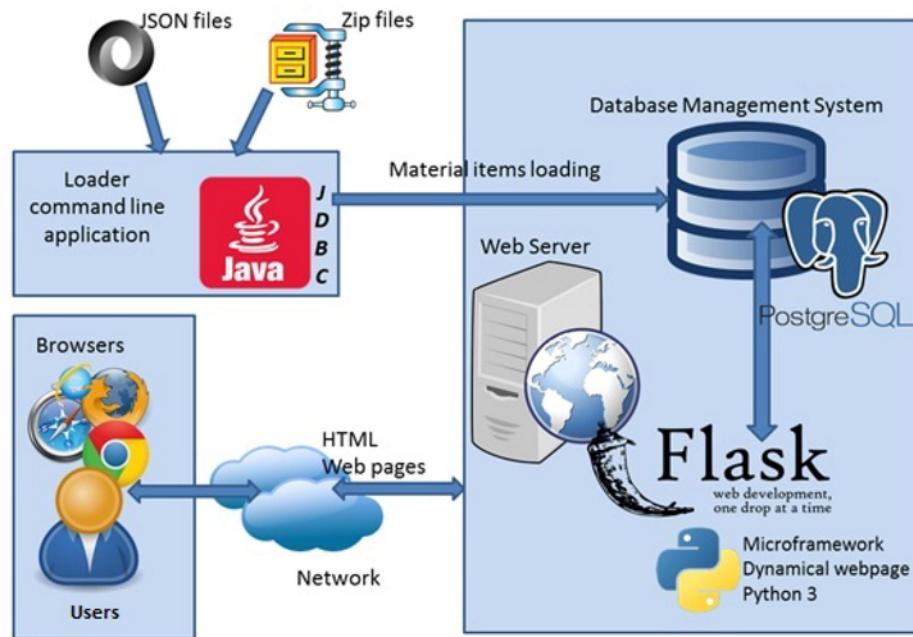
Fig. 1. Workflow of the Novamag database.

Table 1
Summary of the main technologies used in Novamag database.

Technology	Role	More information
PosgreSQL v9.2.3	Relational database to store data	[47]
Python 3.0	Programming language used in Flask	[51]
Flask 0.12.2	Microframewok to build dynamical webpages	[52]
Flask-Bootstrap 3.3.7.1	Flask update for the design of the webpage	[53]
Flask-SQLAlchemy 2.3	Flask update (Object-Relational Mapping)	[54]
PgAdmin III	Tool to control PostgresSQL	[47]
Psql	Console of PostgreSQL	[47]
PyCharm 2017 2.3	Integrated development environment for Python	[55]
JSON	Input data format to import data into the database	[56]
Java 8	Programming language used in the application to import JSON data into PostgreSQL database	[57]
JDBC 3	API to program SQL insertions from Java into the database in the data importation application	[58]
JNDI	Java Naming and Directory Interface to store database connection settings in the data importation application	[59]
Apache Log4j2	Logger in the data importation Java application	[60]
SLF4J	Simple Logging Façade for the data importation Java application	[61]
JUnit 4	Testing framework for Java used in the data importation application	[62]
GitHub	Version control repository used both for the Java data importation application and for the web application	[63]
Eclipse Java Mars	Integrated development environment used in the project for Java programming	[64]

mance. These properties are the maximum energy product $(BH)_{max}$ (related to the maximum magnetostatic energy stored and obtained from the second quadrant of the B(H) hysteresis loop), saturation magnetization M_s (total magnetization that is achieved in a strong external magnetic field H that aligns all magnetic domains), remanence M_r (net magnetization after H is removed) and coercivity H_c (magnetic field that reverses a half of the magnetization reducing the overall magnetization to zero, it determines the "resistance" against demagnetization by external magnetic fields). The larger $(BH)_{max}$, the smaller amount of material is needed to generate a required magnetic field strength, so high values of $(BH)_{max}$ are desired. Energy product and coercivity depend on the magnet's shape due to its own demagnetizing field. The theoretical upper limit of energy product $(BH)_{max}= \mu_0 M_r^2/4$, where μ_0 is vacuum permeability, can be ideally reached for a magnet shape with demagnetizing factor $D = 0.5$ and $H_c > M_r/2$[5]. Extrinsic properties also depend on temperature, in fact they typically decrease as temperature increases, reducing the magnet's performance, especially close to the Curie temperature T_C (i.e. ferromagnetic-paramagnetic transition).

The macroscopic behavior is tightly linked to the microscopic properties called intrinsic. Main magnetic intrinsic properties are atomic magnetic moment μ_{at} (the magnetic moment per volume gives the maximum theoretical M_s), exchange interactions J_{ij} (which determine the magnetic order and T_C) and magnetocrystalline anisotropy K_1 (that can enhance H_c and it is indispensable in modern magnets to get $H_c > M_r/2$)[6]. PMs should have high atomic magnetic moments per volume ($> 0.1\mu_B/\mathring{A}^3$), strong ferromagnetic exchange interactions (able to give $T_C > 600$ K) and high easy axis magnetocrystalline anisotropy ($K_1 > 1$ MJ/m^3) in order to exhibit good extrinsic properties suitable for PM applications. In particular, magnetic materials with hardness parameter $\kappa = \sqrt{K_1/(\mu_0 M_s^2)}>1$ (called "hard" magnets) are very valuable since can be used to make efficient magnets of any shape [6]. At mesoscopic scale, intergranular structure between the grains and crystallographic defects can strongly affect the performance of a magnet [7]. Therefore, the optimization of the material's microstructure is also very important in the design and development of PMs, especially to approach the theoretical upper limit of $(BH)_{max}$[8].

Presently, a magnetic material needs to have quite demanding extrinsic properties in order to be considered as a high-performance PM. Desirable values might be $\mu_0 M_s > 1$ T, $\mu_0 H_c > 1$ T and $(BH)_{max}> 200$ kJ/m^3, with cost lower than 100 \$/kg [9], but it really depends on the specific application [1]. Developing new magnets that fulfill these criteria is quite difficult. For example, it took around 1 century to go from modest Co-steel magnets with $(BH)_{max} = 6$ kJ/m^3 (old fashioned horse-
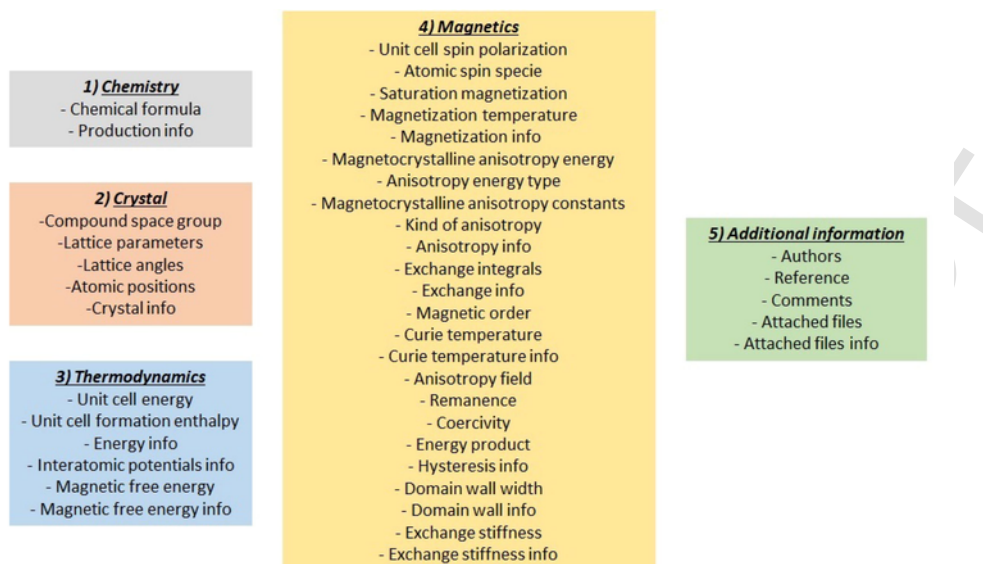
Fig. 2. List of theoretical and experimental properties included in Novamag database.
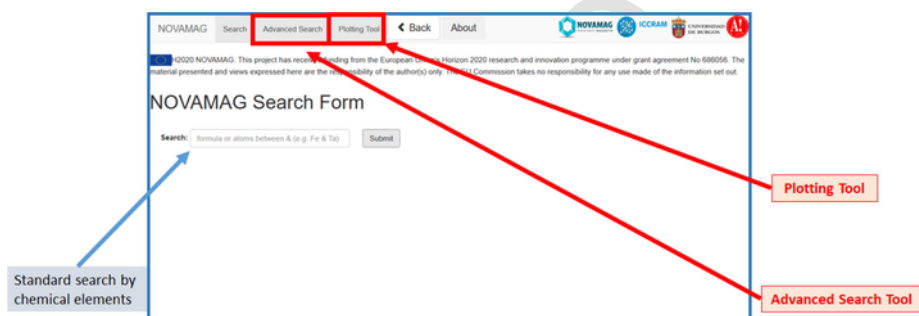

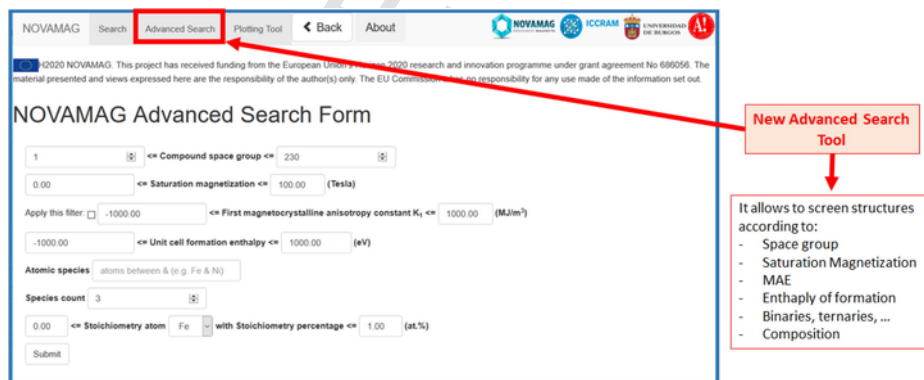**Fig. 3.** Screenshot of the home webpage of Novamag database GUI.

Fig. 4. Screenshot of the advanced search tool of Novamag database GUI.

shoe shape) to current Rare-Earth (RE) based magnets like sintered $Nd_2Fe_{14}B$ with $(BH)_{max} = 470\,kJ/m^3$, which is close to its theoretical upper limit $515\,kJ/m^3$. In fact, $(BH)_{max}$ has not improved much in the past 20 years. The great performance of RE-based PMs makes them essential in many technological applications, leading to a strong dependency on Critical Raw Materials like Nd, Sm or Dy [10]. This situation has forced PM industry to search for other viable alternatives based on RE-free PMs as MnAl(C) τ-phase, FeNi $L1_0$, non-cubic FeCo alloys, MnBi, α''-$Fe_{16}N_2$, exchange spring PM, etc, and also on RE-lean PMs as $NdFe_{12}$[11–14].

Aiming to find new clues, the experimental exploration of new PMs begins to be assisted and guided by computational approaches thanks to their advances in calculation speed, accuracy and reliability [15–18]. In 2011, it was launched the Materials Genome Initiative (MGI) [19–21] alongside the Advanced Manufacturing Partnership to help businesses discover, develop, and deploy new materials by promoting and supporting the third generation of material electronic strucutre databases [22]. As a result, large open material databases with many functionalities, like AFLOW [23,24], the Materials Project [25,26], JARVIS [27,28], etc have been created, providing a powerful tool for discovering and designing novel materials through machine
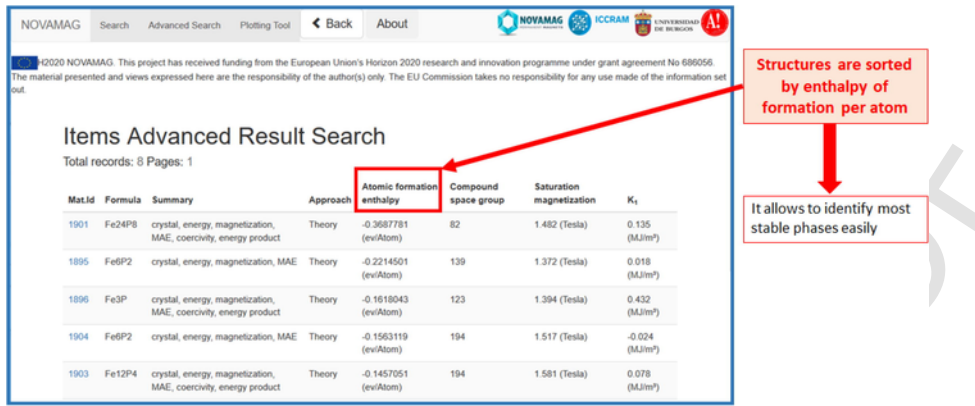
Fig. 5. Screenshot of Novamag database GUI showing the list of materials found in an advanced search. Items are sorted by enthalpy of formation per atom, so that most stable phases can be identified easily.
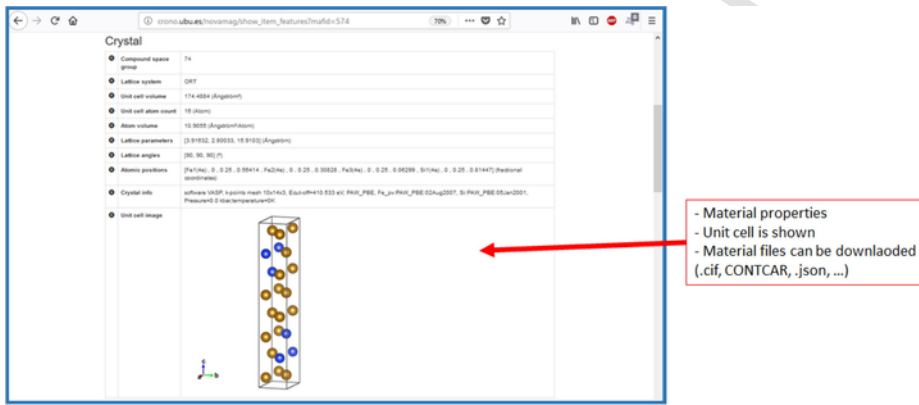

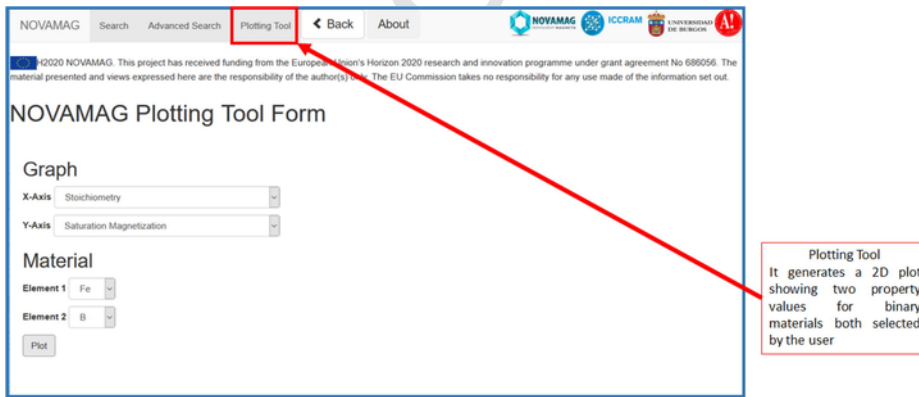**Fig. 6.** Screenshot of Novamag database GUI showing material properties of a selected item.

Fig. 7. Screenshot of Novamag database GUI showing the plotting tool.

learning and data mining techniques [29–32]. Recently, NOMAD repository [33] was established to host, organize, and share materials data. At present, NOMAD contains ab initio electronic structure data from Density Functional Theory (DFT) and methods beyond. Some examples of material properties that have been calculated by high-throughput computational approach are elasticity [34], piezoelectricity [35] and electrolytics [36]. A review of some material databases can be found in Ref. [37]. Concerning to magnetic materials, we highlight the MAGNDATA database [38], that provides more than 500 published commensurate and incommensurate magnetic structures, and MagneticMaterials.org, an online repository of auto-generated magnetic materials databases that makes use of the ChemDataExtractor toolkit to extract magnetic properties automatically from scientific journal articles and the-

ses, e.g. recently an auto-generated materials database of T_C has been created using this approach [39]. For the case of PMs, the NovoMag database [40] shares data of magnetization and magnetocrystalline anisotropy energy (MAE) for some Fe-Co-N ternary compounds [41] and cobalt nitrides [42] predicted through similar methodologies as used in the present work.

Current databases based on MGI like AFLOW or Materials Project provide information of atomic magnetic moment, but other relevant magnetic properties are missing, like MAE, exchange integrals, T_C, coercivity, energy product, etc which are needed for screening and discovering new high-performance Rare-Earth free/lean PMs. In this work, we describe the Novamag database [43] which aims to complement and extend these databases for the case of PMs by making pub-
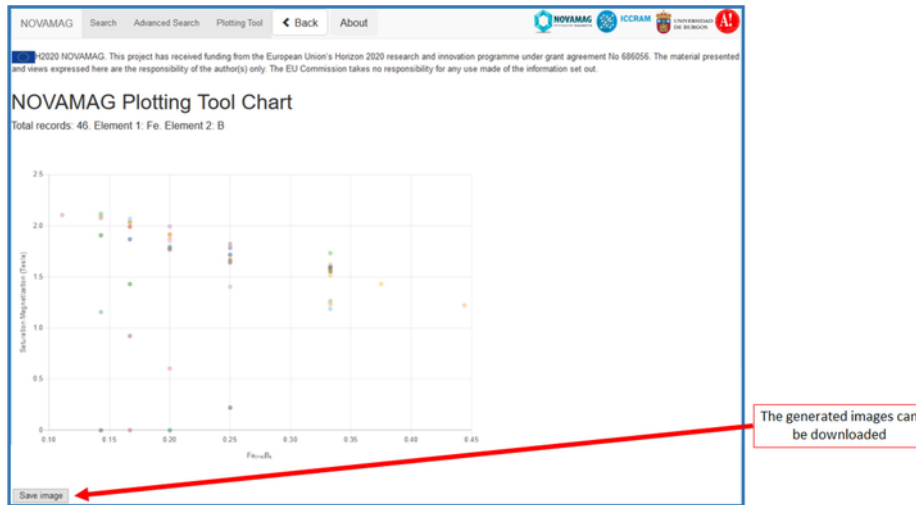
Fig. 8. Screenshot of Novamag database GUI showing a generated image by the plotting tool.
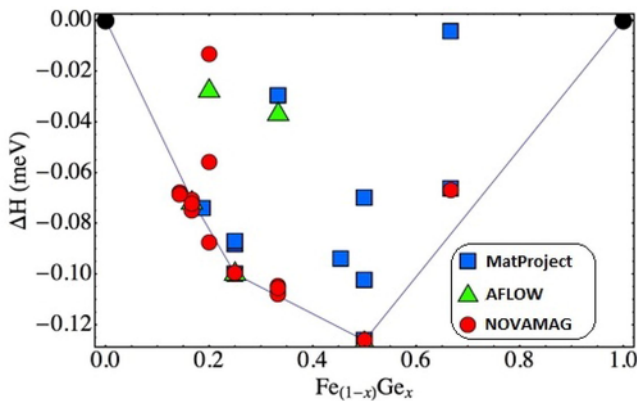

Fig. 9. Calculated formation enthalpy at zero-temperature for some low-energy Fe-Ge metastable phases obtained in Novamag using AGA (red circle), and found in Material databases: Materials Project (blue square) and AFLOW (green triangle). Blue line represents the enthalpy hull line. (For interpretation of the references to colour in this figure legend, the reader is referred to the web version of this article.)

licly available many theoretical and experimental results of magnetic materials studied in the H2020 European project Novamag [44]. This paper is organized as follows: Section 2 explains the software technologies used in the development of the database, while Section 3 gives a detailed tutorial on how to use it. Next, Section 4 shows a general overview of the available data and the methods used to obtain them. In Section 5, we discuss about possible ways to take advantage of Nova-

mag database for exploring the novel promising phases uploaded into it. Finally, this paper ends with a summary of the main conclusions.

2. Methodology

In this section the technologies involved in the development of Novamag database are described. One mandatory requirement present in each decision in the design and implementation of this database is that every component has to be free and widely supported by the community. The application consists of two main modules: i) a web application that uses Phyton ecosystem technologies to show and search the materials and their related information and ii) a data loader application that uses Java ecosystem technologies to insert new items in the database (i.e., Novamag Java Loader Application). These new items are in JSON format. Fig. 1 shows the general workflow of the Novamag database. Both developments are publicly available in two GitHub projects. The Web Application is in Ref. [45], while the Java data loader project is in Ref. [46]. These applications share the same PostgreSQL database [47]. Some of the reasons why PostgreSQL is chosen as the database management system include the following:

- The database schema and data items relationships are simple enough to be represented by a relational system. In fact, the schema consists of a main table (i.e., items) containing almost all information about the materials, and a very small set of tables containing information about chemical composition, attached files, and authors.
- Relational databases are the most extended database systems, and PostgreSQL is one of the most popular. PostgreSQL is an open source
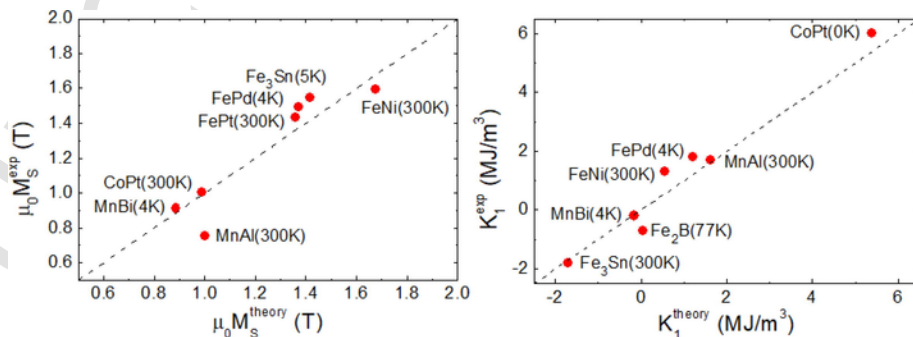

Fig. 10. Experimental and theoretical saturation magnetization (left) and first magnetocrystalline anisotropy constant K_1 (right) of some representative magnets. The experimental temperature is shown in parenthesis, while all theoretical values were calculated with DFT in a high-throughput manner and correspond to T = 0 K. Experimental data are taken from Refs. [67,81–84,14,85,86].
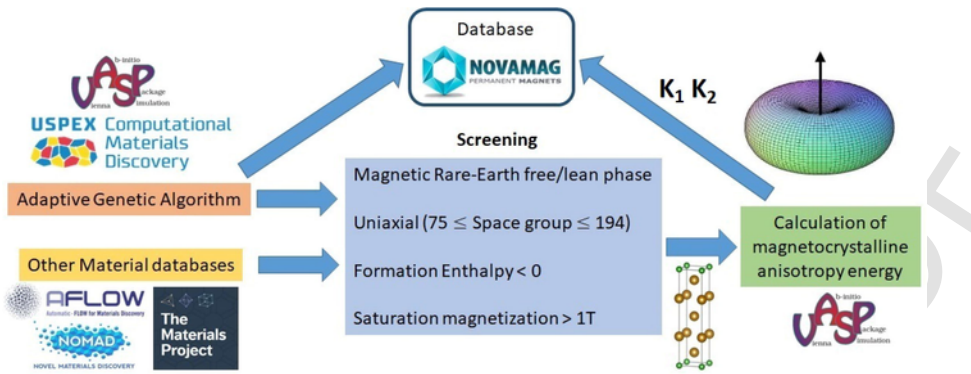
Fig. 11. Workflow of the high-throughput calculation of magnetocrystalline anisotropy energy developed in Novamag project for the discovery of high-performance Rare-Earth-free/lean PMs.
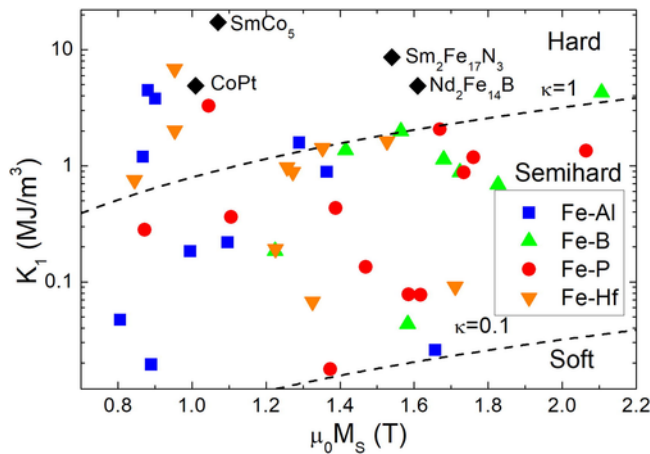

Fig. 12. High-throughput calculation of first anisotropy constant K_1 as a function of polarization $\mu_0 M_s$ for some theoretical uniaxial Fe-based binaries (Fe-X where X = Al, B, P and Hf) with $\Delta H_F < 0$. The dashed lines correspond to magnetic hardness parameter $\kappa = \sqrt{K_1/(\mu_0 M_s^2)}$ for values $\kappa = 1$ and 0.1. Hard magnetic materials ($\kappa > 1$) can be used to make efficient magnets of any shape. Black symbols stand for some known hard phases [2].
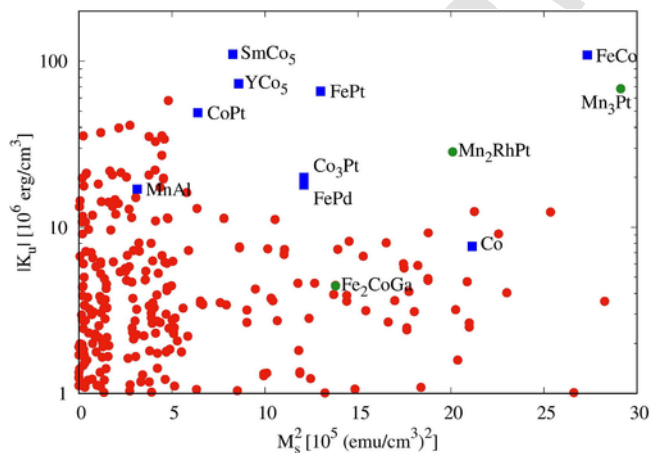

Fig. 13. High-throughput calculation of the first anisotropy constant K_1 as a function of magnetization for stable binary and ternary magnetic materials. The blue squares mark the known experimental compounds, and the green circles denote three promising candidates (Mn_3Pt, Mn_2RhPt, and Fe_2CoGa) identified as PMs. (For interpretation of the references to colour in this figure legend, the reader is referred to the web version of this article.)

database. It has a graphic easy-to-use administration interface and advanced features that are used in the project (i.e., it supports JSON data, triggers, stored procedures and functions). PostgreSQL presents a high level of conformance to SQL standard ANSI/ISO specifications.

The open Novamag database has a Free and Open Source Software (FOSS) licensing and the link to access it is given by Ref. [43].

2.1. The Novamag Java Loader Application

This application is a utility that can read JSON files containing information about one or several materials and load it into the database. The JSON file can reference some attached files, which are supposed to be located in the same path as the JSON file. The application also can cope with zip files containing a subdirectories tree. This subdirectory tree can contain several JSON files and their attached files. Again, the attached files of a JSON file must be located in the same path as the JSON file.

The loader application is invoked by the database administrator from the operative system command line specifying the path of the JSON or ZIP file as a command line argument. Because it is a Java application, it can be invoked both within Unix or Windows operative systems. If remote execution for the database administrator is needed, FTP with SSH for Unix, or a Windows remote terminal for Windows, can be used. JSON format was adopted because the data is presented in form of aggregation. An item can contain several file references, some arrays like MAE, or some more complex data like the atomic positions. XML and JSON are the most extended solutions for this level of complexity in the data representation. XML is a much heavier format than JSON, therefore JSON was considered as the best choice. Presently, efforts are being made to develop a common format for Computational Materials Science Data based on JSON file [33,48].

Nowadays, Java is one of the most widespread programming languages. Given that the Loader Application source code is free and available for the community, a very popular language was needed. Application portability for Linux and Windows without recompilation is another issue that was taken into account when Java was chosen. Java is an Object Oriented language. It is very mature and has a lot of libraries and resources. Once Java was chosen for the development of the loader, many of the rest of technologies were determined by such election (i.e., JDBC, JNDI and JUnit).

A logger was used to record the messages the application throws into a log file. Some messages can be eventual error messages, and some others can be confirmations that everything was performed properly. Apache Log4j is one of the most extended loggers for Java, Log4j2 is its newest version. It is a software from Apache Foundation, so its support over the next years is guaranteed. Even being Log4j a very
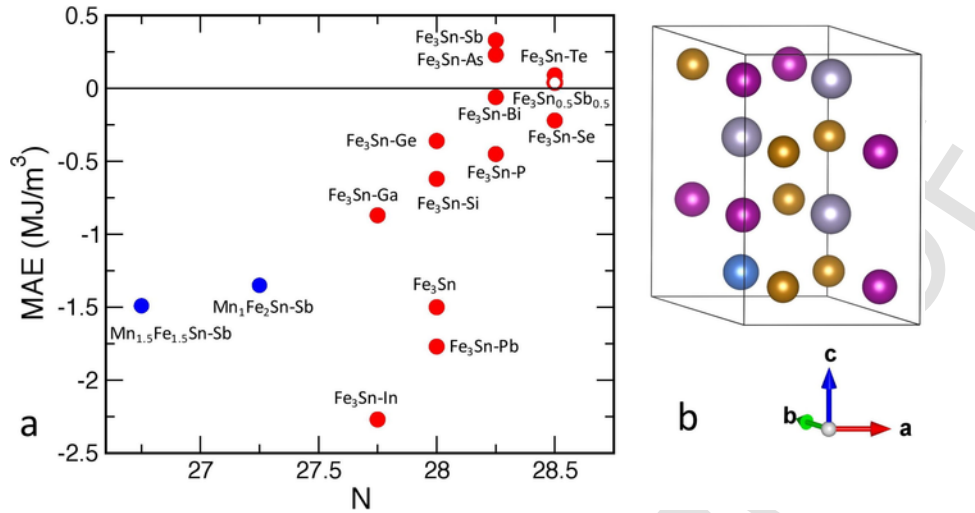
Fig. 14. MAE and crystal structure of the $Fe_yMn_{3-y}Sn_xM_{1-x}$ system, y = 1.5, 2, and 3; x = 0.5, 0.75, and 1. a) The magnetocrystalline anisotropy energy (MAE) calculated from first principles as a function of the number of valence electrons, N, per formula unit. b) The $1 \times 1 \times 2$ Fe_3Sn hexagonal cell with one impurity atom on the tin sublattice. Fe atoms are shown with brown spheres, Sn atoms with grey and M (M = Si, P, Ga, Ge, As, Se, In, Sb, Te, Pb and Bi) impurity atom is shown with the blue sphere. Violet spheres represent the Mn atoms on the Fe sublattice. (For interpretation of the references to colour in this figure legend, the reader is referred to the web version of this article.)
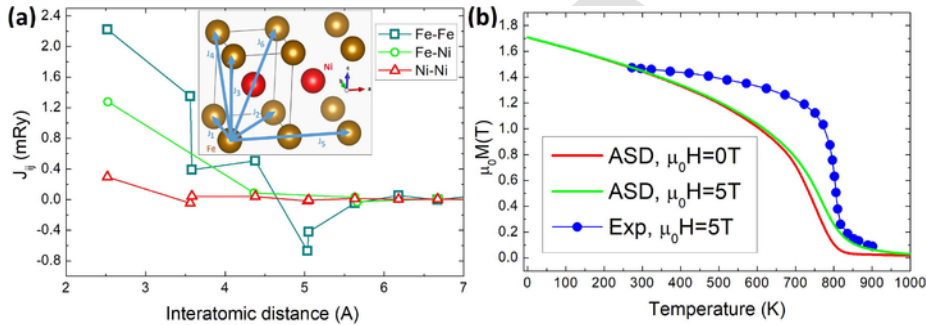
Fig. 15. (a) Estimated exchange integrals of $L1_0$ FeNi as a function of the interatomic distance. Inset shows a diagram of the Fe-Fe exchange parameters up to the sixth nearest neighbour (labelled by J_i i = 1,…,6). (b) Total magnetization versus temperature of $L1_0$ FeNi with no external magnetic field (red line) and external magnetic field μ_0H = 5T (green line), obtained by ASD simulations. Blue circles correspond to experimental data of magnetization with external magnetic field μ_0H = 5T reported in Ref. [106]. (For interpretation of the references to colour in this figure legend, the reader is referred to the web version of this article.)
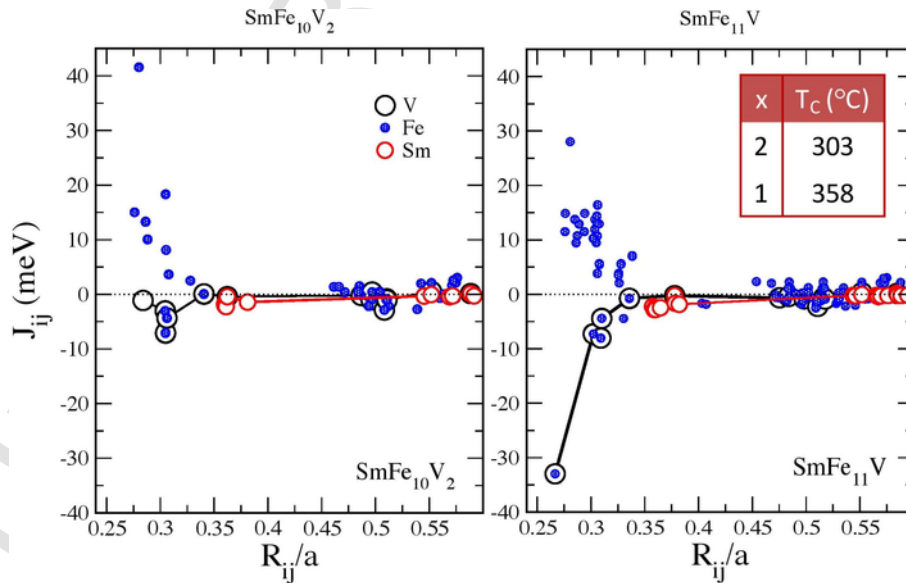
Fig. 16. Inter-site exchange parameters J_{ij} between atoms *i* and *j* separated by the distance R_{ij} of $SmFe_{10}V_2$ (a) and $SmFe_{11}V$ (b) compounds. The J_{ij}s are shown for all R_{ij}s involving i = V, Fe, and Sm (shown by large black, small filled blue, and medium red circles, respectively). *a* stands for the lattice constant. In the inset the mean-field estimation of T_C is given; x stands for the V content, i.e. 2 in $SmFe_{10}V_2$ and 1 in $SmFe_{11}V$.
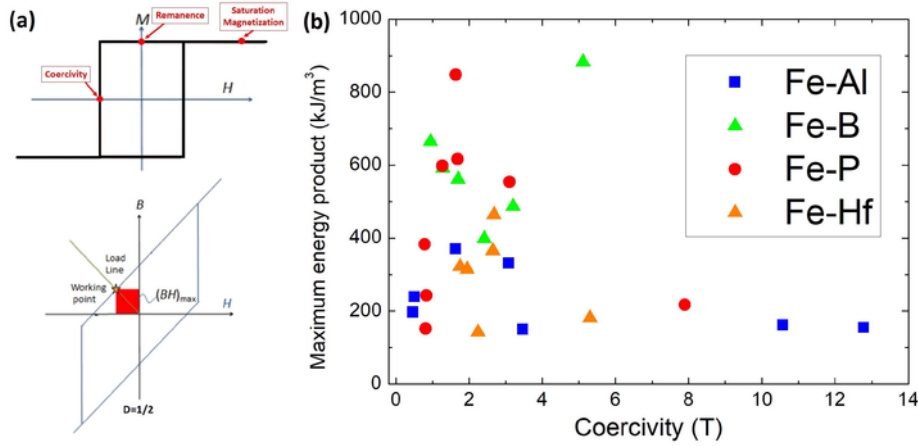
Fig. 17. (a) (top) Perfectly rectangular M(H) loop and (bottom) B(H) loop for obtaining maximum energy product. (b) High-throughput calculation of theoretical maximum energy product $(BH)_{max}$ and maximum coercivity ($H_{C,max} = H_K$) given by the Stoner-Wohlfarth model for the Fe-based binaries showed in Fig. 12 (with $\kappa > 1/2$).
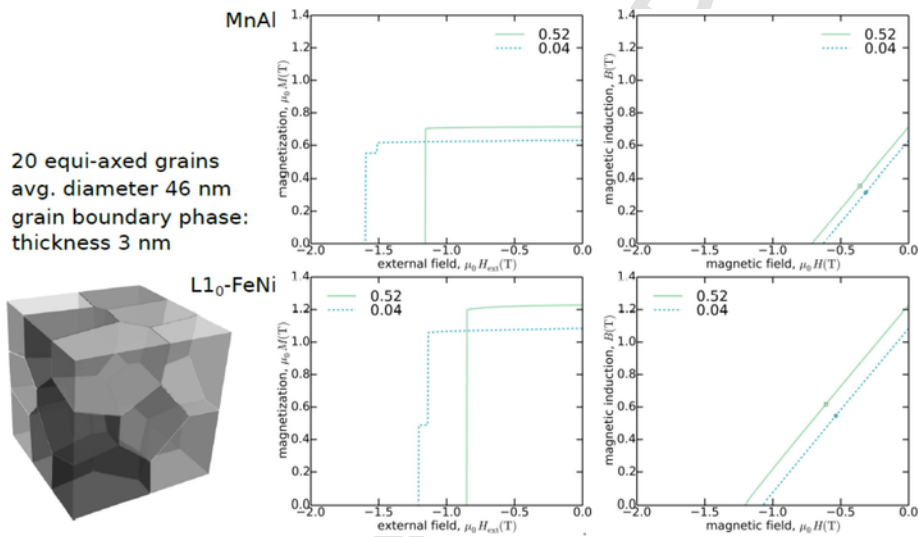
Fig. 18. (Left) Magnets structure with 3 nm thin grain boundary phase. (Mid) For both materials demagnetization curves M over H_{ext} (Right) the corresponding B over H curve.

Table 2
Lattice parameters of the $Fe_{3-x}Mn_xSn_{1-y}Sb_y$ alloys, obtained by Rietveld refinements of the X-ray Diffraction patterns.

| Sample	Space Group	a(Å)	b(Å)	c(Å)
Fe_3Sn	#194, $P6_3/mmc$	5.4621(5)	5.4621(5)	4.3490(6)
$Fe_{2.25}Mn_{0.75}Sn_{0.75}Sb_{0.25}$	#194, $P6_3/mmc$	5.4858(7)	5.4858(7)	4.3721(6)
$Fe_{2.5}Mn_{0.5}Sn_{0.75}Sb_{0.25}$	#194, $P6_3/mmc$	5.5551(1)	5.5551(1)	4.4398(1)
$Fe_2Mn_1Sn_{0.75}Sb_{0.25}$	#194, $P6_3/mmc$	5.5000(4)	5.5000(4)	4.3829(6)
$Fe_{1.5}Mn_{1.5}Sn_{0.75}Sb_{0.25}$	#194, $P6_3/mmc$	5.5338(1)	5.5338(1)	4.4270(2)
$Fe_{1.5}Mn_{1.5}Sn_{0.9}Sb_{0.1}$	#194, $P6_3/mmc$	5.5545(3)	5.5545(3)	4.4453(4)

Fig. 19. Measured values of anisotropy field and saturation magnetization for some experimental magnetic samples included in the Novamag database.

popular logger, SLF4J was used as facade increasing the compatibility with other loggers. That is, the Java loader program only interacts with SLF4J. Then SLF4J receives the Java loader program invocations and translate them into Log4 invocations. In this way, the application does not depend on Log4j and can work in the future with any other logger supported by SLF4J.

Finally, Eclipse was adopted as IDE (Integrated Development Environment) because it is probably the Java most extended IDE. The Mars version was the newest version at the beginning of the development of this application.

Fig. 20. Proposed general strategy to experimentally explore the crystal phase space neighborhood of promising theoretical Fe-based binaries found in the database.

Fig. 21. Strategy to make use of Novamag database for tuning Fe_3Sn phase.
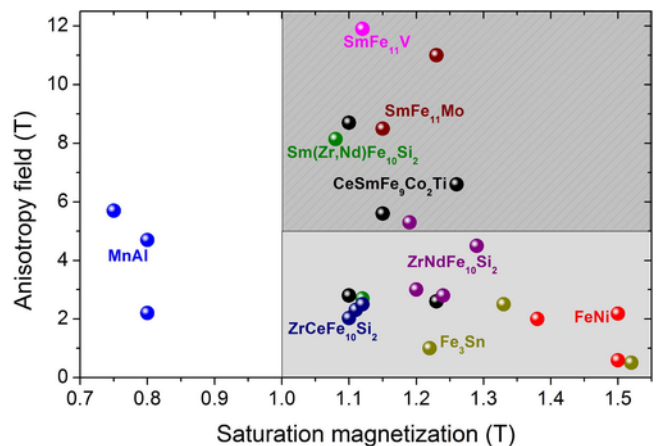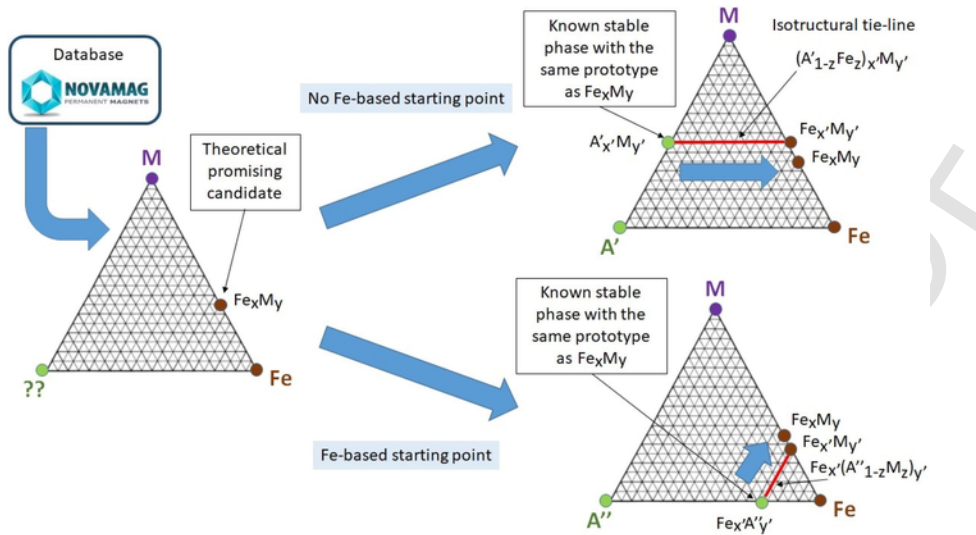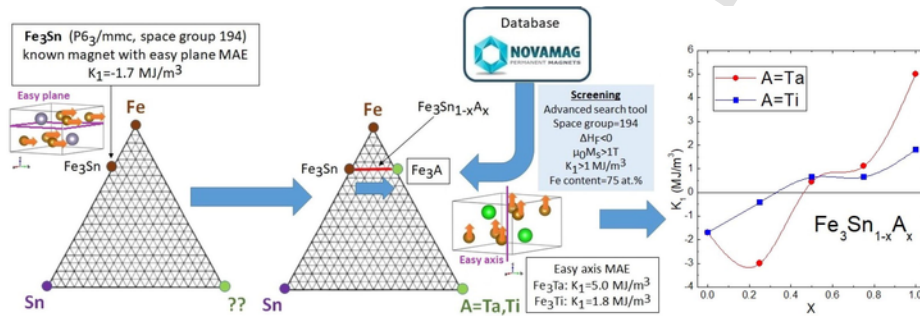
2.2. The Novamag Web Application

The web application allows to query the information available from the previous importation process. It has been developed using a web framework named Flask, which is a microframework for Python based on Werkzeug and Jinja 2, and it is BSD licensed. Python is one of the language with greatest growing in the last years, as can be consulted in the Tiobe Ranking (see Ref. [49]). Their properties make it one of the most powerful programming languages including structured, object-oriented and functional paradigm. On the other hand, the Flask and Python architecture, allows adding new modules in the development in a very simple way.

The dynamic web pages are developed using the Model-View-Presenter design pattern using the following Python/Flask libraries:

- Werkzeug: collection of various utilities for Web Server Gateway Interface (WSGI) applications and has become one of the most advanced WSGI utility modules (Presenter). WSGI is a simple calling convention for web servers to forward requests to web applications or frameworks written in the Python programming language.
- Jinja 2: a modern and designer-friendly templating language for Python, modelled after Django's templates. It is fast, widely used and secure with the optional sandboxed template execution environment (View).
- SQLAlchemy: is the Python SQL toolkit and Object Relational Mapper that gives application developers the full power and flexibility of SQL. It gives data access model with generated SQL from the persistent model in the database (Model).

The web requests are processed by a Werkzeug class, that loads the data and redirect the request to the appropriate Jinja2 template, that renders the HTML dynamically using the previous data. The data are loaded using SQLAlchemy code. All the SQL code is automatically generated from a persistent model extracted from the PostgreSQL schema to Python code, using a tool named sqlacodegen (see Ref. [50]). All the developed code follows this well-known pattern, allowing an easy maintenance and evolution of the code in the future.

From the point of view of the web design, it has been loaded the Flask-Bootstrap package. Bootstrap is an open source toolkit for developing with HTML, CSS, and JS providing a standard and responsive web design. This guarantees a correct and uniform visual design in all the web pages.

All this software has been developed using the PyCharm IDE (Integrated Development Environment), version Professional 2017.3, built on November 28, 2017. The used technologies are all multi-platform, since the product has been developed on Windows, but it is currently deployed and running on Linux. Table 1 provides a summary of the main technologies used in the Novamag database and their role.

2.3. Uploading procedure

In the first stage of the database development, a set of theoretical and experimental properties to be included in the database was agreed by the Novamag consortium. Fig. 2 shows the full list of properties. These properties are classified into 5 categories following MGI standards and the Review of Material Modelling (RoMM) vocabulary: (i)

chemistry, (ii) crystal, (iii) thermodynamics, (iv) magnetics and (v) additional information.

In order to deal and upload the large amount of data generated by computational high-throughput approaches (see Sections 4.1 and 4.2), we created an automated transfer procedure using metadata JSON files written by bash scripting. Once the data is in JSON format it can be uploaded into the database by the Novamag Java Loader Application. A JSON file can contain information of a solely material or of several materials. The attached files of these materials must be allocated in the same path than the JSON file for the loading. The Novamag Java Loader needs several jar libraries that provide methods to manage JSON format, JDBC database connectivity, JNDI services and logging. If a large data upload is needed, then Java Loader Application can cope with ZIP compressed files. The ZIP files can contain a sub-directory tree. In each sub-directory new sub-directories or JSON files can be allocated.

3. Graphical user interface

A friendly Graphical User Interface (GUI) has been developed to use and explore the Novamag database easily. Fig. 3 shows the home webpage of Novamag database, which currently contains two search modes: i) standard and ii) advanced, as well as a plotting tool.

The standard search mode allows to perform quick and general search through the database by specifying the chemical name abbreviation [43]. For example, if one wants to search for compounds with iron and nickel, then one should type "Fe & Ni" inside the box called "Search" and then click on the button "Submit", see Fig. 3. In this case, the system will show all available compounds that contain the specified chemical elements. Additionally, one can search for specific structures by typing the chemical formula, e.g. "FeNi2".

Alternatively, users can also perform advanced search by clicking on the button "Advanced Search" [65], that is placed on the top of home webpage, see Fig. 3. Next, after doing that, it will appear the advanced search site, see Fig. 4. At present, it allows to filter and screen compounds according to: Crystallographic space group symmetry, saturation magnetization (M_s), first magnetocrystalline anisotropy constant (K_1), unit cell formation enthalpy, atomic species, species count and stoichiometry.

These filters are very useful to identify promising materials for PM development in a first screening stage. To this end, we recommend to select uniaxial space groups (from 75 to 194) because they might exhibit a well-defined magnetocrystalline anisotropy easy axis, saturation magnetization above 1 Tesla, negative unit cell formation enthalpy (in order to reject very unstable phases), atomic species like magnetic elements (Fe, Ni, Co) and non-Critical Raw Materials (that could be light elements to induce tetragonal distortions and phase stabilization like B, C, N, P, etc or/and transition metals with high spin-orbit coupling as Ta, Hf, etc), species count (binaries, ternaries, etc) and stoichiometry corresponding to Fe-rich compounds (with Fe content above 50% at.) to enhance saturation magnetization and Curie temperature. Additional filters as Curie temperature, coercivity or maximum energy product can also be useful in a second screening stage, and might be implemented in the future. Some general search strategies through the database are discussed in Section 5.

Once the search settings are ready and submitted, then the list of items that fulfill these criteria are presented, see Fig. 5. By default, items are sorted by enthalpy of formation per atom, so that most stable phases for a given chemical formula can be identified easily. In the list of items, it is shown some properties or fields of each compound in different columns like: material identification number (Mat.Id), chemical formula, summary (data available of each item), approach (theory or experiment), atomic formation enthalpy, space group, saturation magnetization and first magnetocrystalline anisotropy constant.

In order to see more details of a compound that is in the list one should click on the corresponding material identification number (called Mat.Id, at the first column). Then, all available data of this compound will be shown, see Fig. 6. On the left hand side of the name of each field or property, there is a small black icon with label "i", by clicking on it one can see more information about the definition and physical units of that property. Finally, material metadata files like crystallographic information file (.CIF), JSON file used in the database to upload it, CONTCAR (output file of VASP code that describes the relaxed unit cell), figure of the unit in portable network graphics format (.png), etc can be found and downloaded in section "Additional information" (at the end of the webpage of each material).

The GUI also includes a plotting tool [66] that allows to visualize data distribution for analysis purposes. Namely, it generates a 2D plot showing two property values (on X and Y axis, respectively) selected by the user from a given set (Atom volume, Stoichiometry, Compound space group, Atomic formation enthalpy, Atomic energy, Saturation magnetization, First Magnetocrystalline anisotropy constant K_1, Curie temperature, Anisotropy field, Remanence, Coercivity, Energy product, Domain wall width and Exchange stiffness) for materials with chemical elements chosen by the user too. Presently, for the sake of simplicity, this tool only applies to binary systems (note most of the current uploaded items in the database are Fe-based and Co-based binary materials). Users can access to this tool by clicking on the button "Plotting Tool", that is placed on the top of home webpage, see Fig. 7. The generated images can be downloaded as shown in Fig. 8.

Finally, we present a training example of the GUI for the well-known PM: L1$_0$ CoPt [67]. CoPt is widely used as a PM in medical and military applications, as well as in precision instruments where its good performance justifies the high cost [2]. Let's make use the search advanced tool of Novamag database [65] for finding data about this PM. For instance, we can set the following filters: (i) space group = 123, (ii) atomic species = "Co & Pt" (iii) species count = 2 (binary alloy), and (iv) Co content equal to 50 at.%. Doing so, it finds one available item calculated by the methodology described in Section 4.2.1. By clicking on it, one access to crystallographic data as lattice parameters ($a = 2.69234Å, c = 3.71592Å$) and magnetic properties as saturation magnetization ($\mu_0 M_S = 0.988$ T) and MAE ($K_1 = 5.381$ MJ/m^3, $K_2 = 0.114$ MJ/m^3), among others, which are in quite good agreement with experimental data [67], see Fig. 10.

4. Material data available

This section gives a brief overview of the data available in Novamag database. Additional theoretical and experimental contributions from the Novamag consortium, not shown or mentioned here, are expected to be uploaded into the database in the near future.

4.1. Theoretical structures calculated with an Adaptive Genetic Algorithm

One of the most important and difficult step in the computational high-throughput technique for materials design is the prediction of new stable crystal phases [68,69]. Here, we make use of an Adaptive Genetic Algorithm (AGA) [70] to explore the crystal phase space for many Rare-Earth-free/lean magnetic binary and ternary compounds. This task was computationally performed using the software USPEX [71,72] combined with Vienna Ab Initio Simulation Package (VASP) [73–75]. USPEX uses as an input the number and type of ions to be considered within the unit cell only. At the first step, a set of structures is generated at random, by randomly choosing a crystal space group, corresponding lattice vectors, and ion positions. These initial structures are far from their equilibrium, thus performing a structure relaxation is required to estimate accurately the energy of each one, which serves as a fitness criterion. A subset of fitted structures is selected to generate a

next generation of structures by means of genetic operations (crossover and mutations). The process of random generations of structures is performed also at each step to provide a diversity of structures for each generation. The search for an optimal structure is performed until no new best structures are generated for a certain number of generations or the maximum number of generations is reached. We modified and optimized the interface between USPEX and VASP codes in order to improve the performance of structural optimization as well as to perform calculations in a high-throughput manner [76–78].

More precisely, we have run USPEX with the evolutionary algorithm method for 3-D structures and the enthalpy as a fitness criterion. The population size was set to twice the number of atoms in the system and the number of generations to be calculated was set to 40. We used 15 generations for convergence and best 65% of the population size was used for new generation. 45% of new structures were obtained by heredity, 5% by soft-mutations, 5% by lattice mutations, and 45% were randomly generated. For the random generation, we used all space groups except triclinic and monoclinic lattice systems. All VASP calculations were performed with the projector augmented wave (PAW) method [79] and generalized gradient approximation (GGA) in the Perdew, Burke, and Ernzerhof (PBE) form [80] (PBE 5.4 potentials). Best generated structures were fully relaxed until maximum force component became less than 5×10^{-3} eV/Å. We used an automatic k-points generating scheme (scaling factor of 40) and energy cut-off up to 1.4 of the default VASP energy cut-off.

In Novamag project, over 15,000 structures have been calculated with AGA methodology, where we mainly explored Fe-rich binary and ternary compounds without RE-elements. Typically, more than 100 of structures are calculated for a given chemical formula. At the moment, only around 10–20 most stable phases (i.e. with the lowest energy) per chemical formula are being uploaded to the Novamag database. The formation enthalpy of these structures is calculated as (binary phase)

$$\Delta H_F(X_a Y_b) = E(X_a Y_b) - a \cdot E(X) - b \cdot E(Y), \tag{1}$$

where $E(.)$ is the energy, a and b are the number of atoms of X and Y in the formula unit $X_a Y_b$, respectively. Fig. 9 presents calculated formation enthalpy at zero-temperature for some Fe-Ge metastable phases obtained in Novamag using AGA, and found in MGI databases like Materials Project [25,26] and AFLOW [23,24]. We see that AGA is able to find many structures close the enthalpy hull line (blue line), reproducing and extending the data available in other databases based on MGI. Computational phase diagrams like Fig. 9 can be easily generated with the Novamag Plotting Tool [66] by choosing the properties "Stoichiometry" and "Atomic formation enthalpy" on the X and Y axis, respectively.

The amount of generated data of each structure depends on the number of atoms in unit cell and on the number of AGA generations. We may consider as representative a compound with 12 atoms/unit cell, which may generate up to 100 GB of data for 650 structures, or about 150 MB/ structure. We can estimate the overall amount of generated data to be about 2 TB, that are stored and backed-up in office computers, external hard drives and Relational Database (PosgreSQL). A back-up of all data is done every month.

4.2. High-throughput search for structures with high magnetocrystalline anisotropy

One of the key intrinsic properties of modern PMs is MAE because it can greatly increase the coercivity. In this section, we discuss about three computational high-throughput strategies performed in the Novamag project for finding magnetic structures with high easy-axis MAE.

4.2.1. Screening of metastable uniaxial phases from AGA and databases

Only a small amount of phases from the large set of theoretical uniaxial magnetic structures close the enthalpy hull line might exhibit a high easy-axis MAE. Hence, a computational high-throughput approach with a good balance between accuracy and calculation speed is needed in order to analyze them and be able to identify most promising ones. To this end, we devised a script that controls the calculation of MAE in an automated way providing as the input only the atomic position file.

For each structure, DFT calculations are performed in several steps. Firstly, we run a full structural optimization (volume, cell and atomic positions) using VASP code with the PAW method [79], GGA in the PBE form [80] (PBE 5.4 potentials), an energy cut-off up to 1.5 of the default VASP energy cut-off, an electronic convergence criterion of 10^{-7} eV, and maximum force equal to 10^{-3} eV/Å. For the optimized structure, accurate charge density and wave function are calculated for ferromagnetic arrangement of spins via collinear spin-polarized DFT calculations, which will serve as input for non-collinear spin calculations (NCL) [87] with spin–orbit coupling. NCL-calculations are performed in a non-self-consistent manner for a set of polar and azimuthal angles, where the electronic convergence criterion is set to 10^{-9} eV and the automatic k-points mesh is generated with a scaling factor of 60. These code parameters were tuned by testing and reproducing experimental MAE data for a set of representative known magnetic materials, see Fig. 10.

Once the energy of an uniaxial unit cell is calculated, constraining the atomic magnetic moments at different polar angles θ, then first and second anisotropy constants K_1 and K_2 are obtained by fitting the energy data to 2nd order function

$$E(\theta) = K_1 \sin^2\theta + K_2 \sin^4\theta. \tag{2}$$

A final procedure, written by bash scripting, was also prepared to upload the large amount of generated data from this approach to the database automatically. This approach is fed by the crystallographic data of Rare-Earth free/lean theoretical structures predicted by AGA (Section 4.1) and found in open material databases that are previously screened according to space group (only uniaxial phases are considered), formation enthalpy (<0) and saturation magnetization ($\gtrsim$1T), see Fig. 11. As an example, in Fig. 12 we show the high-throughput calculation of first anisotropy constant K_1 at T = 0 K as a function of polarization $\mu_0 M_s$ for some theoretical uniaxial Fe-based binaries (Fe-X where X = Al, B, P and Hf) with $\Delta H_F < 0$ and easy axis, predicted by AGA in Novamag project and found in AFLOW database. We observe this approach is capable to reveal hidden RE-free theoretical phases with hardness parameter $\kappa = \sqrt{K_1/(\mu_0 M_s^2)} > 1$, such as hexagonal P-6m2 FeAl ($\kappa = 2.6$), and tetragonal I4/mmm structures $Fe_{16}B_2$ ($\kappa = 1.1$) and Fe_4Hf_2 ($\kappa = 3.0$). Presently, we have calculated and uploaded over 500 Fe-based and Co-based binaries following this methodology. Note similar images as Fig. 12 can be easily made and analysed through the Novamag Plotting Tool [66] by choosing the properties "Saturation Magnetization" and "First magnetocrystalline anisotropy constant K_1" on the X and Y axis, respectively.

4.2.2. Tetragonally distortion of cubic phases

Enlightened by the work of Burkert *et. al.* on tetragonal FeCo alloys, [88] we have performed high throughput calculations on the tetragonally distorted cubic magnetic materials to screen for candidates as PMs, as shown in Fig. 13. All the binary and ternary compounds with cubic structures including one of Cr, Mn, Fe, Co, and Ni from the Materials Project database [25,26] are considered, where 1% compressive strain is applied to get the tetragonally distorted structures under the constant volume approximation. Presently, around 600 items have

been uploaded following this approach. There are quite a few compounds showing large magnetocrystalline anisotropy induced by the imposed tetragonal distortions. For instance, Mn_3Pt shows an anisotropy as large as $|K_1| = 6.8 \, MJ/m^3$, and Mn_2RhPt with an anisotropy of $|K_1| = 2.8 \, MJ/m^3$. Concerning the sign of K_1, it is noted that compressive and tensile strain will lead to opposite magnetocrystalline anisotropies as the original cubic materials are isotropic to the first order due to the high symmetry. An interesting question is how such tetragonal distortions can be stabilized. We suspect that light interstitial atoms such as H, B, C, and N will lead to substantial tetragonal distortions, as recently investigated in Fe [89] and FeCo [90,91] alloys. Systematic calculations have been performed on compounds with the Cu_3Au (as for Mn_3Pt) and Heusler (as for Mn_2RhPt and Fe_2CoGa) structures with light interstitials, and the results will be reported elsewhere.

4.2.3. Modified magnetic materials from first principles

Another interesting computational high-throughput strategy to find promising PMs is to try different dopants on known magnetic structures in order to tune and improve their properties. For instance, the Novamag database provides data of first principles calculations for the RE-free modified Fe_3Sn compound [92]. Among all the Fe-based intermetallic compounds the Fe_3Sn phase is the most attractive, due to the highest concentration of Fe and therefore high magnetic moment. However, as it has been shown experimentally, the magnetocrystalline anisotropy of this compound is planar [84], while the uniaxial anisotropy is a requirement for a good PM. We have studied the influence of dopants on the magnetocrystalline anisotropy of Fe_3Sn (see Fig. 14 a). On the Sn sublattice we considered 25 at.% of impurities, such as M = Si, P, Ga, Ge, As, Se, In, Sb, Te, Pb, and Bi. On the Fe sublattice Mn was added as a structure stabilizer.

The high temperature phase of Fe_3Sn has a hexagonal crystal structure with space group $P6_3/mmc$ (#194). The $1 \times 1 \times 2$ supercell of Fe_3Sn comprising of 12 Fe and 4 Sn atoms, one of which was substituted by a dopant (see Fig. 14 b) was considered. In the case of doping with Mn, 6 or 4 Fe atoms were substituted. Structures were relaxed using VASP [73–75] within the PAW method [79]. The electronic exchange and correlation effects were treated by the GGA in the PBE form [80]. For the calculation of the magnetic properties the full-potential linear muffin-tin orbital (FP-LMTO) method implemented in the Relativistic Spin Polarized toolkit (RSPt code) [93,94] was used. We performed integration over the Brillouin zone, using the tetrahedron method with Blöchl's correction [95]. The k-point convergence of the MAE for the chosen supercell size was found when increasing the Monkhorst-Pack mesh [96] to $24 \times 24 \times 24$ used in all calculations.

The calculated MAEs were plotted as a function of the number of valence electrons per formula unit for doping atoms on the Sn and Fe sublattices, see Fig. 14. Positive numbers correspond to the uniaxial MAE. The addition of certain elements, such as Sb, As, and Te allowed one to change MAE from planar to uniaxial, however the absolute value was rather small. The maximal uniaxial MAE found (for As and Sb dopants), is obtained for Group VA elements of the periodic table.

Calculated MAE of system with increased Sb content, i.e. $Fe_3Sn_{0.5}Sb_{0.5}$ with 28.5 valence electrons per formula unit, was found to be close to the value for $Fe_3Sn_{0.75}Te_{0.25}$ with the same number of valence electrons (see opaque circle in Fig. 14). Therefore, for this system the MAE depends more on the number of valence electrons rather than on the dopant. It was shown experimentally [92] that the $Fe_3Sn_{0.5}Sb_{0.5}$ system is unstable unless doped with Mn. However, adding Mn to $Fe_3Sn_{0.75}Sb_{0.25}$ system changes anisotropy back to planar. Though the increase of Mn content leads to the increase of absolute value of MAE. More data about the 15 items shown in Fig. 14 are available in the database.

Concerning the consistency between the calculation of MAE performed here with RPSt code and in Sections 4.2.1 and 4.2.2 with VASP code, note the high reproducibility and precision of current DFT codes based on PBE functional framework [18]. For instance, we have calculated intrinsic magnetic properties of Fe_3Sn using both codes (VASP and RPSt) obtaining very similar results and good agreement with experiment, see Figs. 10 and 14[92,84]. Note data available in the database could also be helpful for identifying possible systematic errors between different codes or/and DFT approximations.

4.3. Exchange integrals and Curie temperature

Another important intrinsic property of magnetic materials is the exchange energy, which is typically described by the classical Heisenberg Hamiltonian,

$$E_{ex} = -\frac{1}{2}\sum_{i,j} J_{ij}\mathbf{s}_i \cdot \mathbf{s}_j, \tag{3}$$

where J_{ij} are the exchange parameters and $\mathbf{s}_i$ is the unit vector along the magnetic moment of atom i-th. The factor 1/2 takes care of the double counting in the summation. This is the convention adopted in the database, but note there are many works and codes where Eq. 3 is defined without the factor 1/2, so in these cases the J_{ij} parameters are 2 times smaller than those from Eq. 3. A warning message is displayed in the database's field "exchange info" when a different convention is used in order to avoid any misunderstanding. From J_{ij} one can determine the magnetic order (ferromagnet, antiferromagnet, etc), roughly estimate the T_C using mean-field approximation (MFA) or random phase approximation (RPA), and build atomistic spin dynamics (ASD) models [97–102] to calculate the temperature dependence of magnetic properties (magnetization, domain wall width, exchange stiffness, etc).

4.3.1. Rare-Earth-free compounds

First principles calculations of J_{ij} have been calculated and uploaded to the database for some promising known Rare-Earth free PMs such as MnAl τ-phase X[103] and $L1_0$ FeNi. For instance, Fig. 15a shows the estimated exchange integrals of $L1_0$ FeNi as a function of the interatomic distance using frozen magnon calculations implemented in FLEUR code [98,104,105]. Note FLEUR code follows the definition given by Eq. 3 that includes factor 1/2. We employed the spin spiral formalism with 1960 k-points in the irreducible Brillouin zone (IBZ), plane-wave cut-off of $k_{max} = 4.1$ a.u.$^{-1}$ and 463 q-points in the IBZ. We see that Fe-Fe intralayer exchange interaction is stronger than interlayer one. We also observe that Fe-Ni and Ni-Ni exchange interactions are quite weak, in fact only first nearest neighbour interaction might play a relevant role in the spin dynamics. The Curie temperature given by ASD simulations using these exchange parameters is $T_C = 800$ K, which is in good agreement with experiment [106] (see Fig. 15b). The details of this ASD model and calculation's settings can be found in the database. Note a better agreement of magnetization curve with experiment in the all temperature range can be achieved by rescaling the temperature in the classical ASD simulations [107] or including quantum effects [108,109]. Additionally, the database contains data about exchange stiffness and domain wall width given by ASD models (presently, only for the systems mentioned above), which can be useful for micromagnetics simulations (see Section 4.4.2) within a multiscale modelling approach [110]. We plan to perform these calculations in a high-throughput way in the future.

4.3.2. Rare-Earth-lean 1:12 compounds

Exchange parameters for the known $SmFe_{10}V_2$ system, as well as for the newly stabilized $SmFe_{11}V$ [111] were obtained using Lichtenstein's method [112,113], as implemented in FP-LMTO code RSPt [114]. Note

code RSPt defines Eq. 3 without factor 1/2, so the following results are based on the convention used in this code. The electronic exchange and correlation effects were treated by the generalized gradient approximation (GGA) in the Perdew, Burke, and Ernzerhof (PBE) form [80]. The k-point mesh equal to $18 \times 18 \times 24$ was used in all calculations. In Fig. 16 the calculated J_{ij}s are shown for pairs of atoms ij with i fixed to V, Fe, and Sm, and all corresponding js at distances R_{ij} from the first co-ordination shell up to 0.6 of the lattice constant. As one may see from Fig. 16, the strongest exchange interactions are between Fe atoms that fall off with the distance and are close to zero starting at a distance of approximately 0.35 of the lattice constant. They are positive, i.e. favor the ferromagnetic alignment of magnetic moments on the Fe atoms, and therefore play a dominating role in the paramagnetic-to-ferromagnetic transition and define to a large degree the transition temperature (T_C). The behavior of the Fe-Fe interactions is qualitatively rather similar in both $SmFe_{10}V_2$ and $SmFe_{11}V$ compounds, although the highest values differ by up to 50 % being larger for $SmFe_{11}V$. It is also noticeable that all the V-V as well as all the types of interactions involving Sm are rather weak. The Fe-V interaction at the first coordination shells is, however, relatively large, though around factor 2 weaker than the strongest Fe-Fe interactions in $SmFe_{10}V_2$. In both cases they favor the antiferromagnetic alignment of magnetic moments on the Fe and V atoms. In $SmFe_{10}V_2$, where there are the Fe-V pairs in the first coordination shell, the antiferromagnetic exchange interaction between Fe and V is strong. However, it is well counteracted by the strong Fe-Fe interactions. In the MFA, the T_C can be obtained as follows (not including factor 1/2 in the Heisenberg Hamiltonian):

$$T_C^{MFA} = \frac{2J_0}{3k_B}.$$
(4)

where k_B is the Boltzmann constant. Here T_C is proportional to the on-site exchange parameter J_0 where $J_0 = \Sigma_i J_{0i}$, i.e. the sum over all co-ordination shells. T_Cs are rather similar in both compounds and well above the room temperature. Note that we only took into account Fe interactions for T_C and possible contributions from Sm $4f$ are not included in the approximation since $4f$ are treated as spin-polarized core.

4.4. Extrinsic magnetic properties

4.4.1. Stoner-Wohlfarth model

Once the saturation magnetization (M_S) and magnetocrystalline anisotropy constants (K_1 and K_2) are calculated, it is possible to roughly estimate hysteresis loop properties as coercivity, remanence and maximum energy product by means of the Stoner-Wohlfarth model in the limit of coherent rotation [5]

$$\frac{E}{V} = K_1 \sin^2\theta + K_2 \sin^4\theta$$
$$+ \frac{\mu_0}{4}(1 - 3D)M_S^2 \sin^2\theta - \mu_0 M_S H \cos\theta,$$
(5)

where E is the energy, V is the volume of the material, θ is the angle between magnetization and the easy axis (along z-axis), μ_0 is the vacuum permeability, D is demagnetization factor (which can be a value between 0 and 1) and H is the external magnetic field applied along the easy axis. The first two terms describe the magnetocrystalline energy (discussed in Section 4.2), the third term is the shape anisotropy created by the demagnetizing field of the magnet and the last term is the Zeeman energy. In this model the remanence equals to saturation magnetization (perfectly rectangular hysteresis loop). Here, we define the anisotropy field as the minimum field needed to overcome the magnetocrystalline energy barrier (to reverse magnetization in the absence of shape anisotropy)

$$H_K = \frac{2(K_1 + K_2)}{\mu_0 M_S},$$
(6)

Note that there are other possible definitions [5]. Including the shape anisotropy, the minimum field to reverse the magnetization is the coercivity

$$H_C = \frac{2(K_1 + K_2)}{\mu_0 M_S} + \frac{1}{2}(1 - 3D)M_S^2.$$
(7)

This model describes well nano-size magnetic materials. Taking into account nucleation processes, one arrives to Brown relation

$$H_C \geqslant \frac{2K_1}{\mu_0 M_S} - DM_S.$$
(8)

The value of coercivity corresponding to uniform magnetization reversal by coherent rotation; generally, it is much lower than the anisotropy field, at best about 25% of H_K. On the other hand, the energy product reads [6] $(BH) = \mu_0 D(1 - D)M_S^2$, which is maximum for $D = 1/2$, that is,

$$(BH)_{max} = \frac{1}{4}\mu_0 M_S^2.$$
(9)

Note this value can only be reached if $H_C > M_S/2$ (hardness parameter $\kappa > 1/2$) [6]. The database is being updated with values of magnetic extrinsic properties (remanence, coercivity and maximum energy product) given by the Stoner-Wohlfarth model (see Fig. 17) for structures with easy axis, obtained in the high-throughput calculation of MAE (Section 4.2.1). Similar images as Fig. 17 can be easily made with the Novamag Plotting Tool [66] by choosing the properties "Coercivity" and "Energy Product" on the X and Y axis, respectively.

4.4.2. Micromagnetics

In real magnets, to approach theoretical maximum energy product and coercivity it is essential to have an optimized microstructure [8]. The intergranular structure between the grains plays a significant role determining the magnetic properties, especially if the grain diameter is in the nanometer scale. Hard magnetic phases may be distorted locally near grain boundaries (GBs), because of the different lattice constant of the grain boundary phase. The distorted lattice may give rise to locally different intrinsic magnetic properties. Moreover, surface defects located at GB are sources of strong local demagnetizing fields, which act as nucleation centres. On the other hand, defects close to the GB can pin domain walls during the magnetization's reversal process. Nucleation and pinning mechanisms strongly affect extrinsic properties of hard magnetic phases, as the coercivity [7]. Additionally, intergranular phases modify the exchange coupling behavior between the hard magnetic grains. For instance, nonmagnetic phases eliminate the direct exchange interaction between the hard magnetic grains. Typically, it leads to an increase of the coercive field.

Novamag database contains theoretical results of extrinsic properties calculated with micromagnetic simulations considering optimized microstructures, constructed with the open-source 3D polycrystal generator tool Neper [115], for some of the magnets studied in Novamag project as $Fe_3Sn_{0.75}Sb_{0.25}$, $L1_0$ FeNi, MnAl τ-phase, etc [116]. In Fig. 18 we present demagnetization curves of such MnAl and $L1_0$ FeNi magnets highlighting the influence of different grain boundary magnetizations. As green solid line we show the results of $M_{S,gb} = 0.52 \cdot M_S$ and in blue dotted $M_{S,gb} = 0.04 \cdot M_S$ where M_S is the main phase's saturation magnetization. The structure used for simulating the magnets consists

of 20 equi-axed grains with an average grain size of 46 nm separated by a 3 nm thin layer denoted as the GB phase. With increased magnetization inside the GB phase the coercivity drops by 22% and 16% for MnAl and $L1_0$ FeNi respectively. In Fig. 18 on the right hand side we show the desheared BH loop using a shape factor of 1/3. Computed energy density products for $L1_0$ FeNi range from 230 kJ/m³ to 300 kJ/m³ whereas for MnAl ranges from 80 kJ/m³ to 100 kJ/m³ for high and low saturation magnetization inside the GB, respectively.

4.5. Synthesis and characterization of hard magnetic phase alloys

The computational high-throughput techniques described in previous sections can only approximately estimate the final properties and performance of a real bulk PM. On the other hand, there are also several high-throughput experimental screening techniques as reactive crucible [117] or thin film combinatorial synthesis [118]. However, they allow for a limited number of characterizations and are not representatives of the material in bulk, i.e. of the magnet. Therefore, whether the goal is the manufacture of a magnet, it is necessary to give the processing recipes of the material in bulk for a possible upscaling at an industrial level.

In order to provide this kind of valuable information, the database is being extended with experimental results obtained in Novamag project, such as synthesis routes and the structural and magnetic characterization for CRM-free Fe_3Sn, FeNi and MnAl alloys [119], or the RE-lean $ThMn_{12}$-type tetragonal structure magnetic materials. For instance, Table 2 shows the lattice parameters obtained by Rietveld refinements of the X-ray Diffraction patterns for a set of $Fe_{3-x}Mn_xSn_{1-y}Sb_y$ alloys synthesized by solid-state reaction in the attempt to tune Fe_3Sn alloys [92,120], while Fig. 19 shows a summary of the anisotropy field and M_S obtained in different alloys [121–125]. We see that the alloys can be classified by their magnetic properties. As it is well known, the intrinsic properties of the magnetic alloys suitable for magnets must have high anisotropy field and high M_S (dark grey lined zone) as $SmFe_{11}V$, $SmFe_{11}Mo$ or $SmFe_9Co_2Ti$. Other alloys, which have high M_S, can be further processed in order to increase their anisotropy (light grey zone), as it is the case of Fe_3Sn.

5. Possible strategies to exploit promising theoretical novel phases in the Novamag database

MGI has created a new scenario with many theoretical phases that could be very appealing for different technological applications. However, one of the main challenges in MGI is to find experimental routes to synthesize most promising theoretical materials given by computational high-throughput approaches. From a theoretical point of view, determining the stability and possible synthesis conditions (temperature, pressure, etc.) of a predicted phase is a hard task that requires an accurate calculation of the full phase diagram at finite temperature (free energy) [126,127]. In some cases, even very unstable phases may remain interesting, although direct attempts to synthesize them may not be successful.

In this section, inspired by isostructural tie-lines [86,128], we discuss about some general strategies to design experimental procedures for exploring most promising theoretical materials found in the Novamag database, fully based on their crystallographic data, by doping known stable phases. The main idea is to think about the predicted phases by AGA in a more flexible manner, it means, as a hint or trend. Hence, making a magnet with some crystal and atomic similarities to these structures might be enough to get a good PM. Bearing this in mind, let's consider a given unknown Fe-based binary Fe_xM_y generated by AGA that fulfills all necessary criteria for being a high-performance PM. First step is to search in literature (Handbook of crystallographic data [129] or databases like the Materials Project [25]) for a known

experimental stable binary phase that contains M element but no Fe (no Fe-based binary) $A'_{x'}M_{y'}$ or contains Fe but no M (Fe-based) $Fe_{x'}A''_{y'}$ with the same crystallographic prototype structure as the theoretical Fe_xM_y and also similar stoichiometry. Next, these known stable phases ($A'_{x'}M_{y'}$ or $Fe_{x'}A''_{y'}$) are used as starting point to explore either the ternary line $(A'_{1-z}Fe_z)_{x'}M_{y'}$ or $Fe_{x'}(A''_{1-z}M_z)_{y'}$, that is, doping with Fe or M, respectively. In this way, it is possible to experimentally explore and approach the neighborhood of promising theoretical phase Fe_xM_y, where the compounds in this region with the same crystal structure might have similar properties as Fe_xM_y. Additionally, since this procedure is based on the same prototype structure as Fe_xM_y it could also trigger the formation of this phase locally during the synthesis. Note that the route using a no Fe-based starting point might be more challenging since one needs to dope the ternary with high content of Fe in order to make it ferromagnetic, especially if A' is not Co or Ni. Fig. 20 shows a diagram explaining the above described strategy. Alternately, the selection of optimal substrates for epitaxial growth of these novel theoretical phases could be a way to stabilize them too [130].

The above described strategy can be reversed. For instance, let's consider well-known phase Fe_3Sn ($P6_3/mmc$, space group 194) that exhibits an easy plane MAE. As indicated in Section 4.2.3, in this system it is necessary to find a way to switch MAE from easy plane to easy axis in order to make it suitable for PM applications. To this end, we can use the search advanced tool of Novamag database[65] with the following filters: (i) space group = 194, (ii) negative formation enthalpy $\Delta H_F < 0$, (iii) $\mu_0 M_S > 1$ T, (iv) $K_{1>} 1 \text{ MJ/m}^3$, (v) binary alloy, and (vi) Fe content equal to 75 at.%. Doing so, it found two promising phases Fe_3A with A = Ta,Ti that fulfill these requirements. Hence, it suggests to explore the ternary line $Fe_3Sn_{1-x}A_x$. A preliminary theoretical analysis using DFT calculations, following the steps described in Section 4.2.1, with software VASP [73–75] (PAW method [79] and GGA-PBE [80]) for 1x1x2 supercells (16 atoms) of $Fe_3Sn_{1-x}A_x$ (A = Ti,Ta) shows that replacing 50% of Sn by Ti or Ta in the Fe_3Sn phase might be enough to switch MAE from easy plane to easy axis, see Fig. 21. Obviously, a more detailed analysis of the stability and MAE of these systems are required in order to clarify the role of these dopants on the Fe_3Sn phase, see Section 4.2.3[92]. Finally, concerning the cubic phases in which a tetragonal distortion can induce a large MAE (see Section 4.2.2), we think that adding light interstitial atoms such as H, B, C, and N in these compounds might be a likely way to achieve it in practice [89–91].

6. Conclusions

In summary, based on the philosophy and standards of MGI, we have developed a comprehensive open database of magnetic material parameters that is being updated with many significant theoretical and experimental results from Novamag project. In the design process, efforts have been made to use free software, standard vocabulary and metadata files that might facilitate interoperability with other existing databases. Additionally, its FOSS license maximizes openness and minimizes barriers to software use, dissemination, and follow-on innovation.

Users worldwide can access to crystallographic and magnetic information of many theoretical structures calculated by DFT combined with an AGA. Presently, it is also being updated with the results of a high-throughput calculation of MAE for a large set of uniaxial magnetic structures predicted with AGA, as well as for tetragonally distorted cubic phases and tuned known magnetic materials. In order to illustrate these methods, we have reported some interesting theoretical phases with high MAE and M_S, such as FeAl, $Fe_{16}B_2$ and Fe_4Hf_2, tetragonally distorted Mn_3Pt and Mn_2RhPt, and doped Fe_3Sn.

Examples of available multiscale theoretical and experimental data about other relevant magnetic properties (exchange integrals, T_C,

anisotropy field, coercivity, maximum energy product, etc.) were also shown, which can be helpful for the design of new promising high-performance RE-free/lean PMs. Aiming to link the computational high-throughput results to experiment, we presented some possible strategies to exploit most promising theoretical materials found in the database. Further results from the consortium of Novamag project are expected to be uploaded into the database in the near future, as well as possible new features and improvements.

Data availability

The raw/processed data required to reproduce these findings are available to download from [43].
CRediT authorship contribution statement

References

[1] O. Gutfleisch, M.A. Willard, E. Brück, C.H. Chen, S.G. Sankar, J. Ping Liu, Magnetic materials and devices for the 21st century: stronger, lighter, and more energy efficient, Adv. Mater. 23 (2011) 821–842.

[2] J.M.D. Coey, Magnetism and Magnetic Materials, Cambridge University Press, 2010.

[3] L.H. Lewis, F. Jiménez-Villacorta, Perspectives on permanent magnetic materials for energy conversion and power generation, Metall. Mater. Trans. A 44 (Suppl 1) (2013) 2.

[4] Anja Brumme, Wind Energy Deployment and the Relevance of Rare Earths, Springer, 2014.

[5] R. Skomski, J.M.D. Coey, Permanent Magnetism, Institute of Physics Publishing, 1999.

[6] R. Skomski, J.M.D. Coey, Magnetic anisotropy — how much is enough for a permanent magnet?, Scr. Mater. 112 (2016) 3–8.

[7] H. Kronmüller, M. Fähnle, Micromagnetism and the Microstructure of Ferromagnetic Solids, Cambridge University Press, 2003.

[8] Josef Fidler, Shanmugasundaram Sivarajan, Permanent magnets: microstructure, In: Reference Module in Materials Science and Materials Engineering, Elsevier, 2018.

[9] J.M.D. Coey, New permanent magnets; manganese compounds, J. Phys.: Condens. Matter 26 (2014) 064211.

[10] European Commission, Study on the review of the list of critical raw materials. Critical raw materials factsheets, Publications office of the European Union, Luxembourg, 2017https://doi.org/10.2873/398823.

[11] R.W. McCallum, L.H. Lewis, R. Skomsky, M.J. Kramer, I.E. Anderson, Practical aspects of modern and future permanent magnets, Annu. Rev. Mater. Res. 44 (2014) 451.

[12] M.D. Kuz'min, K.P. Skokov, H. Jian, I. Radulov, O. Gutfleisch, Towards high-performance permanent magnets without rare earths, J. Phys.: Condens. Matter 26 (6) (Jan 2014), 064205.

[13] K.P. Skokov, O. Gutfleisch, Heavy rare earth free, free rare earth and rare earth free magnets – vision and reality, Scr. Mater. 154 (2018) 289–294.

[14] J.M.D. Coey, New permanent magnets; manganese compounds, J. Phys.: Condens. Matter 26 (6) (Jan 2014), 064211.

[15] N. Drebov, A. Martinez-Limia, L. Kunz, A. Gola, T. Shigematsu, T. Eckl, P. Gumbsch, C. Elsässer, Ab initio screening methodology applied to the search for new permanent magnetic materials, New J. Phys. 15 (2013), 125023.

[16] W. Körner, G. Krugel, C. Elsässer, Theoretical screening of intermetallic ThMn$_{12}$-type phases for new hard-magnetic compounds with low rare earth content, Sci. Rep. 6 (2016) 24686.

[17] Stefano Sanvito, Corey Oses, Junkai Xue, Anurag Tiwari, Mario Zic, Thomas Archer, Pelin Tozman, Munuswamy Venkatesan, Michael Coey, Stefano Curtarolo, Accelerated discovery of new magnets in the Heusler alloy family, Sci. Adv. 3 (4) (2017).

[18] Kurt Lejaeghere, Gustav Bihlmayer, Torbjörn Björkman, Peter Blaha, Stefan Blügel, Volker Blum, Damien Caliste, Ivano E. Castelli, Stewart J. Clark, Andrea Dal Corso, Stefano de Gironcoli, Thierry Deutsch, John Kay Dewhurst, Igor Di Marco, Claudia Draxl, Marcin Dułak, Olle Eriksson, José A. Flores-Livas, Kevin F. Garrity, Luigi Genovese, Paolo Giannozzi, Matteo Giantomassi, Stefan Goedecker, Xavier Gonze, Oscar Grånäs, E.K.U. Gross, Andris Gulans, François Gygi, D.R. Hamann, Phil J. Hasnip, N.A.W. Holzwarth, Diana Iuşan, Dominik B. Jochym, François Jollet, Daniel Jones, Georg Kresse, Klaus Koepernik, Emine Küçükbenli, Yaroslav O. Kvashnin, Inka L.M. Locht, Sven Lubeck, Martijn Marsman, Nicola Marzari, Ulrike Nitzsche, Lars Nordström, Taisuke Ozaki, Lorenzo Paulatto, Chris J. Pickard, Ward Poelmans, Matt I.J. Probert, Keith Refson, Manuel Richter, Gian-Marco Rignanese, Santanu Saha, Matthias Scheffler, Martin Schlipf, Karlheinz Schwarz, Sangeeta Sharma, Francesca Tavazza, Patrik Thunström, Alexandre Tkatchenko, Marc Torrent, David Vanderbilt, Michiel J. van Setten, Veronique Van Speybroeck, John M. Wills, Jonathan R. Yates, Guo-Xu Zhang, Stefaan Cottenier, Reproducibility in density functional theory calculations of solids, Science 351 (6280) (2016).

[19] https://www.nist.gov/mgi.

[20] Materials genome initiative strategic plan. executive office of the president of the united states of america, 2014.http://www.nist.gov/mgi/upload/MGI-StrategicPlan-2014.pdf.

[21] X. Qu, et al., Perspective on materials genome, Chin. Sci. Bull. 59 (2014) 1619–1623.

[22] http://gurka.fysik.uu.se/ESP/.

[23] Aflowlib.http://aflowlib.org/.

[24] S. Curtarolo, W. Setyawan, S. Wang, J. Xue, K. Yang, R.H. Taylor, L.J. Nelson, G.L.W. Hart, S. Sanvito, M. Buongiorno-Nardelli, N. Mingo, O. Levy, Aflowlib.org: a distributed materials properties repository from high-throughput ab initio calculations, Comp. Mater. Sci. 58 (2012) 227.

[25] A. Jain, S.P. Ong, G. Hautier, W. Chen, W.D. Richards, S. Dacek, S. Cholia, D. Gunter, D. Skinner, G. Ceder, K.A. Persson, The materials project: a materials genome approach to accelerating materials innovation, APL Mater. 1 (2013), 011002.

[26] The materials project.https://materialsproject.org/.

[27] https://www.ctcms.nist.gov/knc6/JARVIS.html.

[28] Kamal Choudhary, Francesca Tavazza, Convergence and machine learning predictions of Monkhorst-Pack k-points and plane-wave cut-off in high-throughput DFT calculations, Comput. Mater. Sci. 161 (2019) 300–308.

[29] Lu. Wencong, Ruijuan Xiao, Jiong Yang, Hong Li, Wenqing Zhang, Data mining-aided materials discovery and optimization, J. Materiomics 3 (3) (2017) 191–201.

[30] Yue Liu, Tianlu Zhao, Ju. Wangwei, Siqi Shi, Materials discovery and design using machine learning, J. Materiomics 3 (3) (2017) 159–177.

[31] J. Schmidt, M.R.G. Marques, S. Botti, M.A.L. Marques, Recent advances and applications of machine learning in solid-state materials science, Psik Scientific Highlight of the Month 145 (2019).

[32] Tim Mueller, Aaron Gilad Kusne, Rampi Ramprasad, Machine Learning in Materials Science, John Wiley and Sons Ltd, 2016186–273, chapter 4.

[33] https://repository.nomad-coe.eu/.

[34] Maarten de Jong, Wei Chen, Thomas Angsten, Anubhav Jain, Randy Notestine, Anthony Gamst, Marcel Sluiter, Chaitanya Krishna Ande, Sybrand van der Zwaag, Jose J Plata, Cormac Toher, Stefano Curtarolo, Gerbrand Ceder, Kristin A. Persson, Mark Asta, Charting the complete elastic properties of inorganic crystalline compounds, Sci. Data 2 (2015) 03.

[35] Maarten de Jong, Wei Chen, Henry Geerlings, Mark Asta, Kristin Aslaug Persson, A database to enable discovery and design of piezoelectric materials, Sci. Data 2 (2015) 09.

[36] Qu. Xiaohui, Anubhav Jain, Nav Nidhi Rajput, Lei Cheng, Yong Zhang, Shyue Ping Ong, Miriam Brafman, Edward Maginn, Larry A. Curtiss, Kristin A. Persson, The electrolyte genome project: a big data approach in battery materials discovery, Comput. Mater. Sci. 103 (2015) 56–67.

[37] K.T. Butler, et al., Machine learning for molecular and materials science, Nature 559 (2018) 549.

[38] http://webbdcrista1.ehu.es/magndata/.

[39] C.J. Court, J.M. Cole, Auto-generated materials database of Curie and Néel temperatures via semisupervised relationship extraction, Sci. Data 5 (2018), 180111.

[40] https://www.novomag.physics.iastate.edu/structure-database.

[41] Xin Zhao, Cai-Zhuang Wang, Yongxin Yao, Kai-Ming Ho, Large magnetic anisotropy predicted for rare-earth-free Fe$_{16 - x}$Co$_x$N$_2$ alloys, Phys. Rev. B 94 (Dec 2016), 224424.

[42] Xin Zhao, Liqin Ke, Cai-Zhuang Wang, Kai-Ming Ho, Metastable cobalt nitride structures with high magnetic anisotropy for rare-earth free magnets, Phys. Chem. Chem. Phys. 18 (2016) 31680–31690.

[43] http://crono.ubu.es/novamag/.

[44] http://www.novamag.eu/.

[45] https://github.com/rmartico/NOVAMAG-UBU-WEB.

[46] https://github.com/rmartico/NOVAMAG-Java-Loader.

[47] https://www.postgresql.org/.
[48] L.M. Ghiringhelli, C. Carbogno, S. Levchenko, F. Mohamed, G. Huhs, M. Lüders, M. Oliveira, M. Scheffler, Towards a common format for computational materials science data, Psik Scientific Highlight of the Month 131 (2016).
[49] www.tiobe.com.
[50] https://pypi.org/project/sqlacodegen/.
[51] https://www.python.org/download/releases/3.0/.
[52] https://flask.pocoo.org/.
[53] https://pythonhosted.org/Flask-Bootstrap/.
[54] http://flask-sqlalchemy.pocoo.org/2.3/.
[55] https://www.jetbrains.com/pycharm/.
[56] http://www.ecma-international.org/publications/files/ECMA-ST/ECMA-404.pdf.
[57] http://www.oracle.com/technetwork/java/javase/overview/index.html.
[58] https://docs.oracle.com/javase/8/docs/technotes/guides/jdbc/.
[59] https://docs.oracle.com/javase/8/docs/technotes/guides/jndi/index.html.
[60] https://logging.apache.org/log4j/2.x/.
[61] https://www.slf4j.org/.
[62] https://junit.org/junit4/.
[63] https://github.com/.
[64] https://www.eclipse.org/mars/.
[65] http://crono.ubu.es/novamag/advanced_search.
[66] http://crono.ubu.es/novamag/plotting_tool_search.
[67] H. Shima, K. Oikawa, A. Fujita, K. Fukamichi, K. Ishida, Large magnetocrystalline anisotropy energy of l10-type co100–XPTX bulk single crystals prepared under compressive stress, Appl. Phys. Lett. 86 (11) (2005), 112515.
[68] Artem R Oganov, Gabriele Saleh, Alexander G Kvashnin, Computational materials discovery, R. Soc. Chem. (2019).
[69] Susan B. Sinnott, Material design and discovery with computational materials science, J. Vacuum Sci. Technol. A 31 (5) (2013), 050812.
[70] A.R. Oganov, Modern Methods of Crystal Structure Prediction, WILEY-VCH Verlag GmbH and Co. KGaA, Weinheim, 2011.
[71] Andriy O. Lyakhov, Artem R. Oganov, Harold T. Stokes, Qiang Zhu, New developments in evolutionary structure prediction algorithm USPEX, Comput. Phys. Commun. 184 (4) (2013) 1172–1182.
[72] https://uspex-team.org/en.
[73] G. Kresse, J. Hafner, Ab initio molecular dynamics for liquid metals, Phys. Rev. B 47 (Jan 1993) 558–561.
[74] G. Kresse, J. Furthmüller, Efficiency of ab-initio total energy calculations for metals and semiconductors using a plane-wave basis set, Comput. Mater. Sci. 6 (1) (1996) 15–50.
[75] G. Kresse, J. Furthmüller, Efficient iterative schemes for ab initio total-energy calculations using a plane-wave basis set, Phys. Rev. B 54 (Oct 1996) 11169–11186.
[76] S. Arapan, P. Nieves, S. Cuesta-López, A high-throughput exploration of magnetic materials by using structure predicting methods, J. Appl. Phys. 123 (2018) 083904.
[77] P. Nieves, S. Arapan, G.C. Hadjipanayis, D. Niarchos, J.M. Barandiaran, S. Cuesta-López, Applying high-throughput computational techniques for discovering next-generation of permanent magnets, Phys. Status Solidi C 13 (2016) 942–950.
[78] P. Nieves, S. Arapan, S. Cuesta-López, Exploring the crystal structure space of CoFe2P by using adaptive genetic algorithm methods, IEEE Trans. Magn. 53 (2017) 11.
[79] P.E. Blöchl, Projector augmented-wave method, Phys. Rev. B 50 (Dec 1994) 17953–17979.
[80] John P. Perdew, Kieron Burke, Matthias Ernzerhof, Generalized gradient approximation made simple, Phys. Rev. Lett. 77 (Oct 1996) 3865–3868.
[81] H. Shima, K. Oikawa, A. Fujita, K. Fukamichi, K. Ishida, A. Sakuma, Lattice axial ratio and large uniaxial magnetocrystalline anisotropy in $L1_0$-type FePd single crystals prepared under compressive stress, Phys. Rev. B 70 (2004), 224408.
[82] D. Weller, A. Moser, L. Folks, M.E. Best, M.F. Toney, M. Schwickert, J. Thiele, M.F. Doerner, High K_u materials approach to 100 Gbits/in^2, IEEE Trans. Magn. 36 (1) (2000) 10–15.
[83] Akimasa Sakuma, Yuki Manabe, Yohei Kota, First principles calculation of magnetocrystalline anisotropy energy of MnBi and $MnBi_{1-x}Sn_x$, J. Phys. Soc. Jpn. 82 (7) (2013), 073704.
[84] Brian C. Sales, Bayrammurad Saparov, Michael A. McGuire, David J. Singh, David S. Parker, Ferromagnetism of Fe3Sn and Alloys, Sci. Rep. 4 (2014), 7024 EP –, 11.
[85] Takayuki Kojima, Misako Ogiwara, Masaki Mizuguchi, Masato Kotsugi, Tomoyuki Koganezawa, Takumi Ohtsuki, Taka-Yuki Tashiro, Koki Takanashi, Fe-Ni composition dependence of magnetic anisotropy in artificially fabricated $L1_0$-ordered FeNi films, J. Phys.: Condens. Matter 26 (6) (Jan 2014), 064207.
[86] A. Iga, Magnetocrystalline anisotropy in $(Fe_{1-x}Co_x)_2B$ system, Japan J. Appl. Phys. 9 (1970) 415–416.
[87] D. Hobbs, G. Kresse, J. Hafner, Fully unconstrained noncollinear magnetism within the projector augmented-wave method, Phys. Rev. B 62 (Nov 2000) 11556–11570.
[88] Till Burkert, Lars Nordström, Olle Eriksson, Olle Heinonen, Giant magnetic anisotropy in tetragonal FeCo alloys, Phys. Rev. Lett. 93 (Jul 2004) 027203.
[89] Hongbin Zhang, Imants Dirba, Tim Helbig, Lambert Alff, Oliver Gutfleisch, Engineering perpendicular magnetic anisotropy in Fe via interstitial nitrogenation: N choose K, APL Mater. 4 (11) (2016), 116104.
[90] L. Reichel, A. Edström, D. Pohl, J. Rusz, O. Eriksson, L. Schultz, S. Fähler, On the origin of perpendicular magnetic anisotropy in strained Fe–Co(-X) films, J. Phys. D: Appl. Phys. 50 (4) (Jan 2017), 045003.
[91] R. Salikhov, L. Reichel, B. Zingsem, R. Abrudan, A. Edström, D. Thonig, J. Rusz, O. Eriksson, L. Schultz, S. Fähler, M. Farle, U. Wiedwald, Enhanced spin-orbit coupling in tetragonally strained Fe–Co–B films, J. Phys.: Condens. Matter 29 (27) (2017) 275802.
[92] O.Yu. Vekilova, B. Fayyazi, K.P. Skokov, O. Gutfleisch, C. Echevarria-Bonet, J.M. Barandiarán, A. Kovacs, J. Fischbacher, T. Schrefl, O. Eriksson, H.C. Herper, Tuning magnetocrystalline anisotropy of Fe_3Sn by alloying, Phys. Rev. B 99 (2019), 024421.
[93] John M. Wills, Bernard R. Cooper, Synthesis of band and model Hamiltonian theory for hybridizing cerium systems, Phys. Rev. B 36 (Sep 1987) 3809–3823.
[94] J.M. Wills, M. Alouani, P. Andersson, A. Delin, O. Eriksson, O. Grechnyev, Full-potential electronic structure method, Springer Series in Solid State Science, vol. 167, Springer, Berlin, Germany, 2010.
[95] Peter E. Blöchl, O. Jepsen, O.K. Andersen, Improved tetrahedron method for Brillouin-zone integrations, Phys. Rev. B 49 (1994) 16223–16233.
[96] Hendrik J. Monkhorst, James D. Pack, Special points for Brillouin-zone integrations, Phys. Rev. B 13 (Jun 1976) 5188–5192.
[97] O. Eriksson, A. Bergman, L. Bergqvist, J. Hellsvik, Atomistic Spin Dynamics Foundations and Applications, Oxford University Press, 2017.
[98] Ph. Kurz, F. Förster, L. Nordström, G. Bihlmayer, S. Blügel, Ab initio treatment of noncollinear magnets with the full-potential linearized augmented plane wave method, Phys. Rev. B 69 (2004), 024415.
[99] B. Skubic, J. Hellsvik, L. Nordström, O. Eriksson, A method for atomistic spin dynamics simulations: implementation and examples, J. Phys.: Condens. Matter 20 (31) (Jul 2008), 315203.
[100] http://www.physics.uu.se/research/materials-theory/ongoingresearch/uppasd/.
[101] R.F.L. Evans, W.J. Fan, P. Chureemart, T.A. Ostler, M.O.A. Ellis, R.W. Chantrell, Atomistic spin model simulations of magnetic nanomaterials, J. Phys.: Condens. Matter 26 (2014), 103202.
[102] https://vampire.york.ac.uk/.
[103] P. Nieves, S. Arapan, T. Schrefl, S. Cuesta-López, Atomistic spin dynamics simulations of the MnAl τ-phase and its antiphase boundary, Phys. Rev. B 96 (2017), 224411.
[104] A. Jakobsson, P. Mavropoulos, E. Aolu, S. Blügel, M. Leai, B. Sanyal, I. Galanakis, First-principles calculations of exchange interactions, spin waves, and temperature dependence of magnetization in inverse-Heusler-based spin gapless semiconductors, Phys. Rev. B 91 (2015) 174439.
[105] M. Ležaić, Spin-gap Materials from First Principles: Properties and Applications of Half-metallic Ferromagnets, Rheinisch-Westfälischen Technischen Hochschule Aachen (2005), PhD thesis.
[106] L.H. Lewis, F.E. Pinkerton, N. Bordeaux, A. Mubarok, E. Poirier, J.I. Goldstein, R. Skomski, K. Barmak, De magnete et meteorite: cosmically motivated materials, IEEE Magn. Lett. 5 (2014) 1–4.
[107] R.F.L. Evans, U. Atxitia, R.W. Chantrel, Quantitative simulation of temperature-dependent magnetization dynamics and equilibrium properties of elemental ferromagnets, Phys. Rev. B 91 (2015), 144425.
[108] C.H. Woo, A.A. Semenov, Haohua Wen, S.L. Dudarev, Pui-Wai Ma, Quantum heat bath for spin-lattice dynamics, Phys. Rev. B 91 (2015), 104306.
[109] F. Körmann, A. Dick, T. Hickel, J. Neugebauer, Role of spin quantization in determining the thermodynamic properties of magnetic transition metals, Phys. Rev. B 83 (2011), 165114.
[110] N. Kazantseva, D. Hinzke, U. Nowak, R.W. Chantrell, U. Atxitia, O. Chubykalo-Fesenko, Towards multiscale modeling of magnetic materials: simulations of FePt, Phys. Rev. B 77 (2008), 184428.
[111] A.M. Schönhöbel, R. Madugundo, O.Yu. Vekilova, O. Eriksson, H.C. Herper, J.M. Barandiarán, G.C. Hadjipanayis, Intrinsic magnetic properties of SmFe12-xV_x alloys with reduced V-concentration, J. Alloy. Compd. 786 (2019) 969–974.
[112] M.I. Katsnelson, A.I. Lichtenstein, First-principles calculations of magnetic interactions in correlated systems, Phys. Rev. B 61 (Apr 2000) 8906–8912.
[113] A.I. Liechtenstein, M.I. Katsnelson, V.P. Antropov, V.A. Gubanov, Local spin density functional approach to the theory of exchange interactions in ferromagnetic metals and alloys, J. Magn. Magn. Mater. 67 (1) (1987) 65–74.
[114] Y.O. Kvashnin, O. Grånäs, I. Di Marco, M.I. Katsnelson, A.I. Lichtenstein, O. Eriksson, Exchange parameters of strongly correlated materials: extraction from spin-polarized density functional theory plus dynamical mean-field theory, Phys. Rev. B 91 (Mar 2015), 125133.
[115] R. Quey, P.R. Dawson, F. Barbe, Large-scale 3d random polycrystals for the finite element method: generation, meshing and remeshing, Comput. Methods Appl. Mech. Eng. 200 (2011) 1729–1745.
[116] A. Kovacs, J. Fischbacher, M. Gusenbauer, H. Oezelt, H.C. Herper, O.Y. Vekilova, P. Nieves, S. Arapan, T. Schrefl, Computational Design of the Rare-Earth Reduced Permanent Magnets, In: Engineering, Proceedings of the REMP2018 Conference, 2018.
[117] B. Fayyazi, K.P. Skokov, T. Faske, D.Y. Karpenkov, W. Donner, O. Gutfleisch, Bulk combinatorial analysis for searching new rare-earth free permanent magnets: reactive crucible melting applied to the Fe-Sn binary system, Acta Mater. 141 (2017) 434–443.
[118] G. Giannopoulos, G. Barucca, A. Kaidatzis, V. Psycharis, R. Salikhov, M. Farle, E. Koutsouflakis, D. Niarchos, A. Mehta, M. Scuderi, G. Nicotra, C. Spinella, S. Laureti, G. Varvaro, $L1_0$-FeNi films on Au-Cu-Ni buffer-layer: a high-throughput combinatorial study, Sci. Rep. 8 (2018) 15919.
[119] V. Popov, A. Koptyug, I. Radulov, F. Maccari, G. Muller, Prospects of additive manufacturing of rare-earth and non-rare-earth permanent magnets, Procedia Manuf. 21 (2018) 100–108.

[120] C. Echevarria-Bonet, N. Iglesias, J.S. Garitaonandia, D. Salazar, G.C. Hadji-panayis, J.M. Barandiaran, Structural and magnetic properties of hexagonal Fe_3Sn prepared by non-equilibrium techniques, J. Alloy. Compd. 769 (2018) 843–847.

[121] A. Martin-Cid, A.M. Gabay, D. Salazar, J.M. Barandiaran, G.C. Hadjipanayis, Tetragonal Ce-based Ce-Sm(Fe Co, Ti)$_{12}$ alloys for permanent magnets, Phys. Status Solidi Curr. Top. Solid State Phys. (2016) 15919.

[122] A. Martin-Cid, D. Salazar, A.M. Schönhöbel, J.S. Garitaonandia, J.M. Barandiaran, G.C. Hadjipanayis, Magnetic properties and phase stability of tetragonal $Ce_{1-x}Sm_xFe_9Co_2Ti$ 1:12 phase for permanent magnets, J. Alloys Compd. 749 (2018) 640–644.

[123] A.M. Gabay, A. Martín-Cid, J.M. Barandiaran, D. Salazar, G.C. Hadjipanayis, Low-cost $Ce_{1-x}Sm_x(Fe,Co,Ti)_{12}$ alloys for permanent magnets, AIP Adv. 6 (2016), 056015.

[124] D. Salazar, A. Martín-Cid, J.S. Garitaonandia, T.C. Hansen, J.M. Barandiaran, G.C. Hadjipanayis, Role of Ce substitution in the magneto-crystalline anisotropy of tetragonal $ZrFe_{10}Si_2$, J. Alloys Compd. 766 (2018) 291–296.

[125] R. Madugundo, N.V. Rama Rao, A.M. Schönhöbel, D. Salazar, A.A. El-Gendy, Recent developments in nanostructured permanent magnet materials and their processing methods, Magn. Nanostructured Mater. (2018) 157–198.

[126] R. Lizárraga, F. Pan, L. Bergqvist, E. Holmström, Z. Gercsi, L. Vitos, First principles theory of the hcp-fcc phase transition in Cobalt, Sci. Rep. 7 (2017) 3778.

[127] Xin Zhao, Shu Yu, Shunqing Wu, Manh Cuong Nguyen, Cai-Zhuang Wang, Kai-Ming Ho, Structures, phase transitions, and magnetic properties of Co_3Si from first-principles calculations, Phys. Rev. B 96 (2017), 024422.

[128] P.H. Spriggs, An investigation of the variation of lattice parameters with composition along the tie-line Ni_3P-Fe_3P, Phil. Mag. 21 (1970) 173.

[129] P. Villars, K. Cenzual, R. Gladyshevskii, Handbook of Inorganic Substances 2017, De Gruyter, 2017.

[130] H. Ding, S.S. Dwaraknath, L. Garten, P. Ndione, D. Ginley, K.A. Persson, Computational approach for epitaxial polymorph stabilization through substrate selection, ACS Appl. Mater. Interfaces 8 (20) (2016) 13086–13093.